

# Energy Flux into Internal Lee Waves: Sensitivity to Future Climate Changes Using Linear Theory and a Climate Model

ANGÉLIQUE MELET

*Program in Atmospheric and Oceanic Sciences, Princeton University, Princeton, New Jersey,  
and LEGOS, UMR5566, CNES, CNRS, IRD, Université Paul Sabatier, Toulouse, France*

ROBERT HALLBERG

*NOAA/Geophysical Fluid Dynamics Laboratory, Princeton, New Jersey*

ALISTAIR ADCROFT

*NOAA/Geophysical Fluid Dynamics Laboratory, Princeton University, Princeton, New Jersey*

MAXIM NIKURASHIN

*Institute for Marine and Antarctic Studies, University of Tasmania, and ARC Centre of Excellence  
for Climate System Science, Hobart, Tasmania, Australia*

SONYA LEGG

*NOAA/Geophysical Fluid Dynamics Laboratory, Princeton University, Princeton, New Jersey*

(Manuscript received 18 June 2014, in final form 28 November 2014)

## ABSTRACT

Internal lee waves generated by geostrophic flows over rough topography are thought to be a significant energy sink for eddies and energy source for deep ocean mixing. The sensitivity of the energy flux into lee waves from preindustrial, present, and possible future climate conditions is explored in this study using linear theory. The bottom stratification and geostrophic velocity fields needed for the calculation of the energy flux into lee waves are provided by Geophysical Fluid Dynamics Laboratory's global coupled ocean–ice–atmosphere model, CM2G. The unresolved mesoscale eddy energy is parameterized as a function of the large-scale available potential energy. Simulations using historical and representative concentration pathway (RCP) scenarios were performed over the 1861–2200 period. The diagnostics herein suggest a decrease of the global energy flux into lee waves on the order of 20% from preindustrial to future climate conditions under the RCP8.5 scenario. In the Southern Ocean, the energy flux into lee waves exhibits a clear annual cycle with maximum values in austral winter. The long-term decrease of the global energy flux into lee waves and the annual cycle of the energy flux in the Southern Ocean are mostly due to changes in bottom velocity.

## 1. Introduction

The momentum transferred from the winds to the ocean is the main driver of the large-scale ocean circulation. The wind power input into geostrophic flows, estimated to be of  $O(1)$  TW (Wunsch 1998; Scott and Xu

2009), is then mostly transferred to geostrophic eddies through baroclinic instability (Wunsch and Ferrari 2004). The pathways ultimately leading to the eddy energy dissipation remain uncertain, and several processes can act to dissipate eddy energy in the ocean (Wunsch and Ferrari 2004; Ferrari and Wunsch 2009). Among them are bottom drag (Arbic and Flierl 2004), with an estimated dissipation of 0.2–0.8 TW (Sen et al. 2008), dissipation in the western boundary of the oceanic basins, accounting for an estimated dissipation of 0.1–0.3 TW poleward of 10°N/S (Zhai et al. 2010), and the

---

*Corresponding author address:* Angélique Melet, Geophysical Fluid Dynamics Laboratory, 201 Forrestal Road, Princeton, NJ 08540.

E-mail: angelique.melet@noaa.gov

generation and subsequent dissipation of internal lee waves (e.g., Naveira Garabato et al. 2004; Marshall and Naveira Garabato 2008; Nikurashin and Ferrari 2010b; Nikurashin et al. 2013), with an estimated dissipation of 0.2–0.4 TW (Nikurashin and Ferrari 2011; Scott et al. 2011). The latter is the focus of this paper.

Lee waves can be generated in a stratified fluid through the interaction of deep geostrophic currents with small-scale rough topography (e.g., Bell 1975; St. Laurent and Garrett 2002; Nikurashin and Ferrari 2010b). Analytical calculations of the energy flux into lee waves based on the linear theory of Bell (1975) have been performed recently by Nikurashin and Ferrari (2011) and Scott et al. (2011). The two independent estimates are consistent, with a global conversion rate of 0.2–0.4 TW dominated by the Southern Ocean, which has strong deep reaching currents such as the Antarctic Circumpolar Current (ACC) and where the wind power input into the ocean is greatest. Another recent calculation of the global energy flux into lee waves, performed by Wright et al. (2014), based on in situ data for the bottom currents, suggests a higher global conversion rate of  $0.75 \pm 0.19$  TW, but also with a prominent role of the Southern Ocean.

When lee waves break due to shear or convective instabilities, the energy converted from geostrophic motions into lee waves is dissipated and a fraction of it goes into turbulent mixing in the deep ocean (e.g., Naveira Garabato et al. 2004; Nikurashin et al. 2013). How far from their generation site and how high in the water column lee waves dissipate their energy is largely unknown (e.g., Melet et al. 2014). Lee waves also extract momentum and vorticity from the geostrophic flows through wave drag (Naveira Garabato et al. 2013). Over recent years, the potentially pivotal role of lee waves for the energy budget and dynamical balance of the Southern Ocean has been highlighted in several studies (e.g., Kunze et al. 2006; Nikurashin and Ferrari 2010a; Trossman et al. 2013; Naveira Garabato et al. 2013). Gille et al. (2000) reported from satellite observations that the dissipation of mesoscale eddy energy was partially determined by the roughness of the bottom topography, and hypothesized the underlying process to be the conversion of mesoscale eddy energy into lee waves. Studies based on in situ observations have indeed identified lee-wave-driven mixing as the likely mechanism leading to intense turbulent diapycnal mixing and energy dissipation common throughout areas of rough bottom topography under the ACC, such as the Kerguelen Plateau (Polzin and Firing 1997; Waterman et al. 2013) and the Drake Passage and Scotia Sea (Heywood et al. 2002; Naveira Garabato et al. 2004; Sloyan 2005; St. Laurent et al. 2012; Sheen et al. 2013; Brearley et al. 2013). Diapycnal mixing in the deep ocean sustained by breaking

internal waves (such as internal tides and lee waves) is of importance for large-scale climate since it plays a crucial role for the maintenance of the stable stratification of the deep ocean through a downward diffusive heat flux. Consequently, internal-wave-driven mixing is a key driver of the global overturning circulation (e.g., Talley 2013) and is also pivotal for determining the ocean sequestration of heat and carbon (e.g., Bryan 1987; Park and Bryan 2000; Sokolov et al. 2003; Gnanadesikan et al. 2003, 2004; Wunsch and Ferrari 2004; Friedrich et al. 2011).

However, internal-wave-driven mixing occurs on scales too small for global ocean models to explicitly resolve, and has to be parameterized. Over the last decade, efforts have been focused on parameterizations of the generation and dissipation of internal tides (e.g., Jayne and St. Laurent 2001; Polzin 2009; Decloedt and Luther 2010; Melet et al. 2013), which are the most energetic class of internal waves [with  $O(1)$  TW of energy being dissipated in the deep ocean]. Although the global energy conversion rate in the deep ocean into lee waves is small compared to that into internal tides, the spatial distributions of the energy flux into internal tides and lee waves are strikingly different: lee waves are mostly generated in the Southern Ocean where the energy conversion into internal tides is weak (Nycander 2005; Nikurashin and Ferrari 2011). As it has recently been shown that lee-wave-driven mixing has the potential to impact the ocean state in a climate model (Melet et al. 2014), the energy budget of the ocean eddies, and the large-scale circulation (Trossman et al. 2013), as well as the deep ocean turbulent mixing (Gille et al. 2000; Ito and Marshall 2008; Saenko et al. 2012; Nikurashin and Ferrari 2013), parameterizing lee-wave-driven mixing in climate models warrants serious consideration (MacKinnon 2013).

In most contemporary climate models (using an ocean component at  $1^\circ$  to a  $1/4^\circ$  resolution), geostrophic eddies cannot be resolved in most parts of the ocean (Hallberg 2013) and eddy effects need to be parameterized. The extraction of available potential energy from the mean state by eddies (and corresponding flattening of isopycnal surfaces) is commonly parameterized via a Laplacian diffusion of the height of isopycnal surfaces, using variants of the Gent and McWilliams (1990) scheme. In this approach, eddy energy is implicitly assumed to be dissipated adiabatically, and does not maintain diapycnal mixing. In such models, the strength of the abyssal meridional overturning circulation (MOC) generally decreases with increasing winds over the Southern Ocean. This is not only due to the lack of eddy–mean flow and eddy–convection interactions (Booth and Kamenkovich 2008; Ivchenko et al. 2014), but also to the lack of a coupling between winds and mixing notably through lee waves (Saenko et al. 2012). However, a recent modeling study by

Stanley and Saenko (2014) shows that if a fraction of the parameterized eddy energy is allowed to maintain diapycnal mixing in the deep ocean, then the abyssal MOC generally strengthens in response to an increase of wind energy input in the ocean. In that case, increasing the winds steepens isopycnal surfaces, increases the available potential energy and energy of parameterized eddies, and therefore increases diapycnal mixing in the deep ocean. In their study, using a wind-power-dependent diapycnal diffusivity was key to allowing the abyssal MOC to intensify with increasing winds.

Therefore, the building literature on lee waves and their impact on the ocean and climate calls for a full coupling between the wind power, stratification, parameterized eddies, and lee-wave-driven mixing in climate models. The parameterization proposed by Stanley and Saenko (2014) is the first prescribing deep internal-wave-driven mixing with a dependence on wind strength and eddy energy. To summarize, their “E-conserving” scheme assumes that a fraction of the Gent and McWilliams (1990) parameterized mesoscale eddy energy is transferred to lee waves whose breaking maintains diapycnal mixing. The dissipation rate of the corresponding lee waves is parameterized as the sum of a local turbulent dissipation rate, which corresponds to a fraction of the local dissipation of the waves, and a background value set by the global average of the remaining lee wave energy that is assumed to be dissipated remotely. The dissipation is finally prescribed to decay exponentially above the sea floor, as in the St. Laurent et al. (2002) formulation. Although the mechanism coupling the wind power to diapycnal mixing in the deep ocean was assumed in their study to be the conversion of mesoscale eddy energy into lee waves and their subsequent breaking, the parameterization proposed by Stanley and Saenko (2014) does not physically take into account the generation of lee waves. Notably, whereas linear theory predicts that only topographic features with wavenumbers in the range  $f/U$  to  $N/U$  can radiate lee waves ( $f$  being the Coriolis frequency,  $N$  the buoyancy frequency, and  $U$  the magnitude of the bottom velocity), the Stanley and Saenko (2014) parameterization omits this necessary condition on the topographic roughness scales. Furthermore, the generation and subsequent dissipation of lee waves by geostrophic motions large enough to be resolved in a climate model (such as the ACC) is disregarded. As a result, the spatial distribution of the energy source for deep ocean mixing in their study is completely different than that of the energy flux into lee waves computed by

Nikurashin and Ferrari (2011) and Scott et al. (2011). Finally, the framework proposed by Stanley and Saenko (2014) does not directly take into account the direct feedback of lee-wave-driven mixing on the parameterized eddies. Therefore, progress remains to be made for explicitly and physically coupling the wind power, stratification, parameterized eddies, and lee-wave-driven mixing in climate models.

The present study focuses on the evolution of the lee wave energy flux with changes in hydrography, which represents a step toward a physically based, energetically consistent, and fully interactive coupling of the wind power, stratification, and lee-wave-driven mixing in climate models. We first examine the sensitivity of the rate of generation of lee waves to changes in hydrography that are consistent with the evolution of the ocean state from preindustrial to present and future climate conditions (until year 2200). The analytical calculations of the rate of generation of lee waves are based on linear wave theory of Bell (1975) formulated in terms of the effective topographic spectrum by Nikurashin and Ferrari (2010b, 2011) and summarized in section 2a. The primary challenge to calculate the energy flux into lee waves in climate models is the knowledge of the bottom velocity field, since geostrophic eddies cannot be resolved everywhere (notably in the Southern Ocean, which dominates the generation of lee waves) in contemporary global ocean models, even at  $1/12^\circ$  resolution (Hallberg 2013). Therefore, in these models, the geostrophic bottom velocity needs to be parameterized. The parameterization of the mesoscale eddy kinetic energy used in this paper is based on the work by Marshall and Adcroft (2010) and depends on the modeled available potential energy. This parameterization is presented in section 2b and evaluated in a climate model (presented in section 2c) in section 2d. The sensitivity of the rate of generation of lee waves to changes in hydrography and bottom speed from preindustrial to future conditions is presented in section 3.

## 2. Methodology

### a. Linear theory

An analytical expression for the energy flux  $E_f$  converted from the geostrophic flows into lee waves has been derived from the linear theory of internal waves by Bell (1975) in the limit of subcritical slopes (i.e., when the slope of the topography is smaller than the slope of the radiated lee wave beam):

$$E_f = \frac{\rho_0}{4\pi^2} \int_{-\infty}^{\infty} \int_{-\infty}^{\infty} P(k, l) \frac{\mathbf{U} \cdot \mathbf{k}}{\mathbf{k}} \sqrt{N^2 - (\mathbf{U} \cdot \mathbf{k})^2} \cdot \sqrt{(\mathbf{U} \cdot \mathbf{k})^2 - f^2} dk dl, \quad (1)$$

where  $\rho_0$  is a reference seawater density,  $\mathbf{k} = (k, l)$  is the topographic wavenumber vector,  $P(k, l)$  is the topographic spectrum,  $\mathbf{U}$  is the bottom velocity,  $N$  is the bottom stratification, and  $f$  is the Coriolis parameter. As shown in [Nikurashin and Ferrari \(2011\)](#), (1) can be rewritten in a reference frame rotated at each location along and across the mean flow  $\mathbf{U}$ :

$$E_f = \frac{\rho_0 |\mathbf{U}|}{\pi} \int_{|f|/|\mathbf{U}|}^{N/|\mathbf{U}|} P_*(k) \sqrt{N^2 - |\mathbf{U}|^2 k^2} \sqrt{|\mathbf{U}|^2 k^2 - f^2} dk, \quad (2)$$

where the effective topographic spectrum  $P_*$  is given by

$$P_*(k) = \frac{1}{2\pi} \int_{-\infty}^{\infty} \frac{|k|}{|\mathbf{k}|} P(k, l) dl. \quad (3)$$

The effective topographic spectrum can be related to a one-dimensional spectrum representing topographic scales typical of the lee wave radiative range. At these scales, of  $O(0.1\text{--}10)$  km, abyssal hills dominate the structure of the sea floor. Direct observations of abyssal hills are not available on a global scale, but a parametric representation of the abyssal hill topography spectrum has been derived by [Goff and Jordan \(1988\)](#). If we further assume that abyssal hill topography is isotropic and that lee waves radiate from topographic scales such that  $k \gg k_0$ , with  $k_0$  the characteristic wavenumber at which the abyssal hill spectrum changes from flat to roll-off shape (corner

wavenumber), then the [Goff and Jordan \(1988\)](#) model spectrum can be reduced to a 1D spectrum  $P_{1D}(k)$ :

$$P_{1D}(k) = P_0 k^{1-\mu}, \quad (4)$$

where  $P_0$  is the spectral level and  $1 - \mu$  the spectral slope. While the assumption of isotropy in the topographic spectrum does not strongly impact the estimate of the global energy flux into lee waves ([Nikurashin and Ferrari 2011](#); [Scott et al. 2011](#)), taking into account abyssal hill anisotropy will likely make the estimate of lee wave radiation more accurate in some regions. The second assumption  $k \gg k_0$  is not very restrictive as lee waves are radiated from abyssal hills, with wavelengths  $k^{-1}$  of  $O(0.1\text{--}10)$  km, while  $k_0^{-1}$  is of  $O(50)$  km.

The two parameters  $P_0$  and  $1 - \mu$  are estimated as in [Nikurashin and Ferrari \(2011\)](#) on a  $3^\circ \times 3^\circ$  grid by fitting the model spectrum of [Goff and Jordan \(1988\)](#) to the spectrum estimated from the single beam acoustic data from the U.S. National Geophysical Data Center in a least squares sense in the 2–20-km wavelength range, characteristic of the lee wave radiative range. As shown in [Nikurashin and Ferrari \(2010a\)](#), (3) can be related to (4) following

$$P_*(k) = P_{1D}(k) \frac{B[1/2, (\mu - 1)/2]}{B[1/2, \mu/2]}, \quad (5)$$

where  $B$  is the beta function.

The energy flux based on the linear theory then follows:

$$E_f = \frac{\rho_0 |\mathbf{U}| P_0}{\pi} \frac{B[1/2, (\mu - 1)/2]}{B[1/2, \mu/2]} \int_{|f|/|\mathbf{U}|}^{N/|\mathbf{U}|} k^{1-\mu} \sqrt{N^2 - |\mathbf{U}|^2 k^2} \sqrt{|\mathbf{U}|^2 k^2 - f^2} dk. \quad (6)$$

The linear theory (6) is formally valid for subcritical slopes only, that is, for slopes where the steepness parameter  $\epsilon$  is smaller than a critical value  $\epsilon_c$ , with

$$\epsilon = \frac{N\sqrt{2}h_{\text{rms}}}{|\mathbf{U}|}, \quad (7)$$

and  $h_{\text{rms}}$  is the topographic roughness leading to the radiation of lee waves, calculated from the integral of the topographic spectrum (4) over the radiative lee wave wavelengths:

$$h_{\text{rms}}^2 = \frac{1}{2\pi} P_0 \frac{1}{2-\mu} \left[ \frac{N^{2-\mu} - |f|^{2-\mu}}{|\mathbf{U}|^{2-\mu}} \right]. \quad (8)$$

Over subcritical slopes, linear theory predicts that the energy flux increases as a function of the squared steepness parameter. Over supercritical slopes (when  $\epsilon > \epsilon_c$ ), geostrophic flows are partly blocked by topography and the energy flux saturates instead of increasing with  $\epsilon^2$ . Following [Nikurashin and Ferrari \(2011\)](#), the energy flux into lee waves is therefore corrected for the saturation of the energy flux at supercritical slopes by multiplying the expression given by the linear theory by  $(\epsilon_c/\epsilon)^2$  where  $\epsilon > \epsilon_c$ , and using  $\epsilon_c = 0.7$ .

Thereafter, the energy flux based on the linear theory is therefore calculated using the same analytical expression as in [Nikurashin and Ferrari \(2011\)](#):

$$E_f = \frac{\rho_0 |\mathbf{U}| P_0}{\pi} \frac{B[1/2, (\mu - 1)/2]}{B[1/2, \mu/2]} \int_{|f|/|\mathbf{U}|}^{N/|\mathbf{U}|} k^{-\mu+1} \sqrt{N^2 - |\mathbf{U}|^2 k^2} \sqrt{|\mathbf{U}|^2 k^2 - f^2} dk \min\left(1, \left[\frac{\epsilon_c}{\epsilon}\right]^2\right). \quad (9)$$

### b. Parameterization of the mesoscale eddy velocity

The geostrophic bottom velocity field is needed to compute the energy flux into lee waves. Since climate models do not resolve the mesoscale eddy field globally, the eddy field is parameterized based on the studies of [Eden and Greatbatch \(2008\)](#) and [Marshall and Adcroft \(2010\)](#). In the parameterization, the intensity of eddy activity is predicted in the model using a 2D equation for the mesoscale eddy kinetic energy (MEKE, denoted  $E$  below). The MEKE framework expresses an energy budget in which mean flow energy is removed by mesoscale eddies and the accumulated eddy energy is subsequently dissipated through different mechanisms. The budget of  $E$  is given by

$$\frac{\partial E}{\partial t} = \text{Src} - \gamma E - \frac{C_d \alpha |\mathbf{U}_E|}{H} E + \frac{1}{H} \nabla \cdot (H \kappa_E \nabla E), \quad (10)$$

where the first term of the RHS is the source term for  $E$  [see (11)] and the second is a damping term (here,  $\gamma = 10^{-7} \text{ s}^{-1}$ ). The third term is an energy sink through bottom drag, with  $\alpha$  being a ratio of the 2D mesoscale eddy velocity ( $\mathbf{U}_E$ ) and the bottom mesoscale eddy velocity,  $H$  the ocean depth, and  $C_d$  the drag coefficient set to 0.003 here. The fourth term is the divergence of a flux that represents propagation and spreading of  $E$ , here parameterized as a diffusion. This approach differs from [Eden and Greatbatch \(2008\)](#) by considering the depth integrated eddy energy equation in an attempt to represent the gravest mode unresolved geostrophic turbulence. The source term is diagnosed as the extraction of energy by eddy parameterization due to [Gent and McWilliams \(1990\)](#) and/or the lateral viscosity ([Eden and Greatbatch 2008](#)):

$$\text{Src} = \frac{1}{H} \int_{-H}^{\eta} K_{\text{int}} |s|^2 |N|^2 dz - \frac{0.001}{H} \int_{-H}^{\eta} \mathbf{u} \cdot (\nabla \cdot \boldsymbol{\tau}_{\text{visc}}) dz, \quad (11)$$

where  $|s|$  is the magnitude of the isoneutral slope and  $K_{\text{int}}$  is the thickness diffusivity, both used in the [Gent and McWilliams \(1990\)](#) parameterization, and  $\boldsymbol{\tau}_{\text{visc}}$  is the lateral stress tensor. The factor of 0.001 in (11) is an (assumed small) efficiency for the conversion of energy extracted by horizontal viscosity into baroclinic eddy energy. In practice, the MEKE source terms evolve on baroclinic time scales so that (10) is often near a balanced state in which the slowly changing source terms are balanced by some diffusive smoothing and the faster local damping. This balanced state for MEKE is an augmentation of the closure for eddy energy given by [Cessi \(2008\)](#).

An eddy thickness diffusivity is estimated using a mixing-length scaling,  $\kappa_E \sim LU_E$  (e.g., [Taylor 1915](#); [Bates et al. 2014](#), and references therein). The length scale  $L$  is the smaller of the grid size and the first-mode baroclinic

deformation radius and the predicted eddy energy is used to estimate the velocity scale ( $U_E = \sqrt{2E}$ ), resulting in

$$\kappa_E = 0.03L\sqrt{2E}, \quad (12)$$

where the nondimensional coefficient has been empirically determined.

This eddy parameterization provides a 2D field for the mesoscale eddy velocities where the lee wave parameterization requires a bottom velocity. Because the MEKE parameterization is depth integrated and is targeting the gravest mode eddy structures, we assume that the bottom velocity is simply proportional to the amplitude of those gravest modes (namely  $\alpha U_E$ ), which is consistent with the dissipation term used in the energy Eq. (10). Note that  $\alpha$  is set here to 0.1 so that 1) the interface height diffusivity inferred from MEKE is consistent with the interface height diffusivity used in the model [(12) involves  $\alpha$  through (10)], 2) the total bottom velocity of the coarse-resolution model is consistent with the bottom velocity of a high-resolution model, and 3) the global energy flux into lee waves computed from the linear theory and using the model bottom stratification and speed (including the MEKE contribution) is consistent with previous estimates of the energy flux into lee waves ([Nikurashin and Ferrari 2011](#); [Scott et al. 2011](#)) (see section 2d herein for an evaluation of the MEKE-derived interface height diffusivities and bottom speed in the model).

### c. Climate model description

Calculations of the energy flux into lee waves involve the velocities and buoyancy frequency at the bottom of the ocean. These variables are taken from GFDL's CM2G ocean-ice-atmosphere coupled model used for the IPCC Fifth Assessment Report (AR5) suite ([Dunne et al. 2012](#)). The ocean component is the GOLD isopycnal model ([Hallberg and Adcroft 2009](#)), with a nominal resolution of  $1^\circ$ . The meridional resolution increases toward  $1/2^\circ$  poleward of  $60^\circ\text{S}$  and toward  $1/3^\circ$  equatorward of  $20^\circ$ , and 63 isopycnal layers are used. Standard simulations of CM2G use a Laplacian diffusion operator for the along-isopycnal tracer mixing and an isopycnal height diffusion parameterization, analogous to [Gent and McWilliams \(1990\)](#). In this study, the simulations were performed using the MEKE parameterization in a diagnostic passive mode. These simulations were initialized using a spun-up state of CM2G after 1000 years of integration with year 1860 concentrations of aerosols and greenhouse gases. The first simulation, referred to as pi-control, corresponds to the control run and uses preindustrial (year 1860) concentrations of aerosols and greenhouse gases. The historical simulation has been integrated from the spun-up state using historical

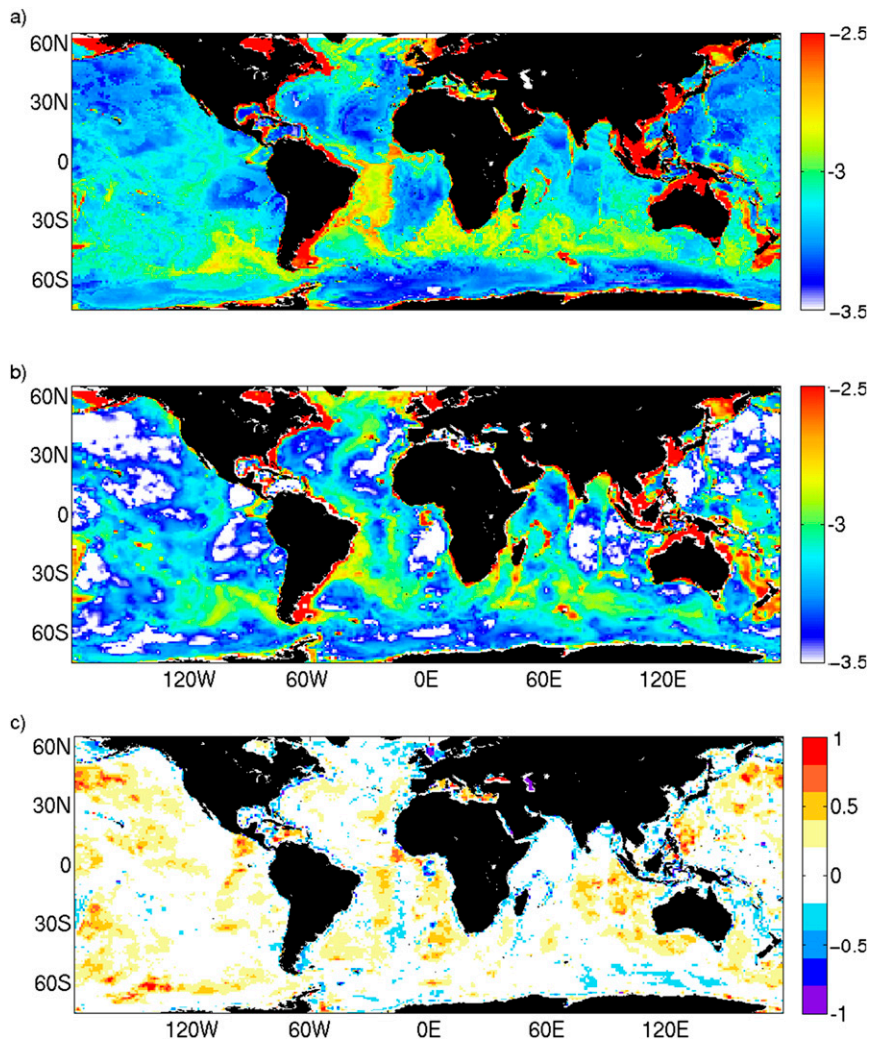


FIG. 1. Bottom stratification from (a) the historical simulation 2000–08 mean (computed from monthly outputs) and (b) WOCE hydrographic atlas, in  $\log_{10}$  scale. Units are  $\text{in s}^{-1}$ . (c)  $\text{Log}_{10}$  of the ratio of the climate model historical 2000–08 mean bottom stratification [(a)] over the WOCE bottom stratification [(b)].

concentrations of aerosols and greenhouse gases over the 1861–2009 period. Projections have been performed until 2200 using the Climate Model Intercomparison Project phase 5 (CMIP5) RCP 2.6, 4.5, 6.0, and 8.5 scenarios for the concentrations of aerosols and greenhouse gases (leading to a radiative forcing peaking at  $\sim 3 \text{ W m}^{-2}$  before 2100 and then declining for RCP2.6, to a radiative forcing of  $\sim 4.5$  and  $\sim 6.0 \text{ W m}^{-2}$  at stabilization after 2100 for RCP4.5 and RCP6.0 respectively, and to a radiative forcing greater than  $8.5 \text{ W m}^{-2}$  in 2100 for RCP8.5).

#### d. Evaluation of the modeled bottom stratification and speed

The rate of conversion of the energy flux into lee waves directly depends on the bottom stratification and

speed simulated by the climate model. CM2G represents overflows, and therefore the bottom stratification, particularly well. The 2000–08 mean bottom stratification of the historical simulation, the bottom stratification of the WOCE hydrographic atlas [Gouretski and Koltermann 2004; computed as in Nikurashin and Ferrari (2011)] and their ratio are shown in Fig. 1. CM2G reproduces the large-scale patterns of the observed bottom stratification, notably in the Southern Ocean where the energy flux into lee waves is large (Fig. 1).

The bottom velocity due to unresolved mesoscale eddies is diagnosed in the model from the MEKE scheme. To ensure that the mesoscale eddy kinetic energy diagnosed from the MEKE scheme is broadly consistent with the ocean state in the simulation, the

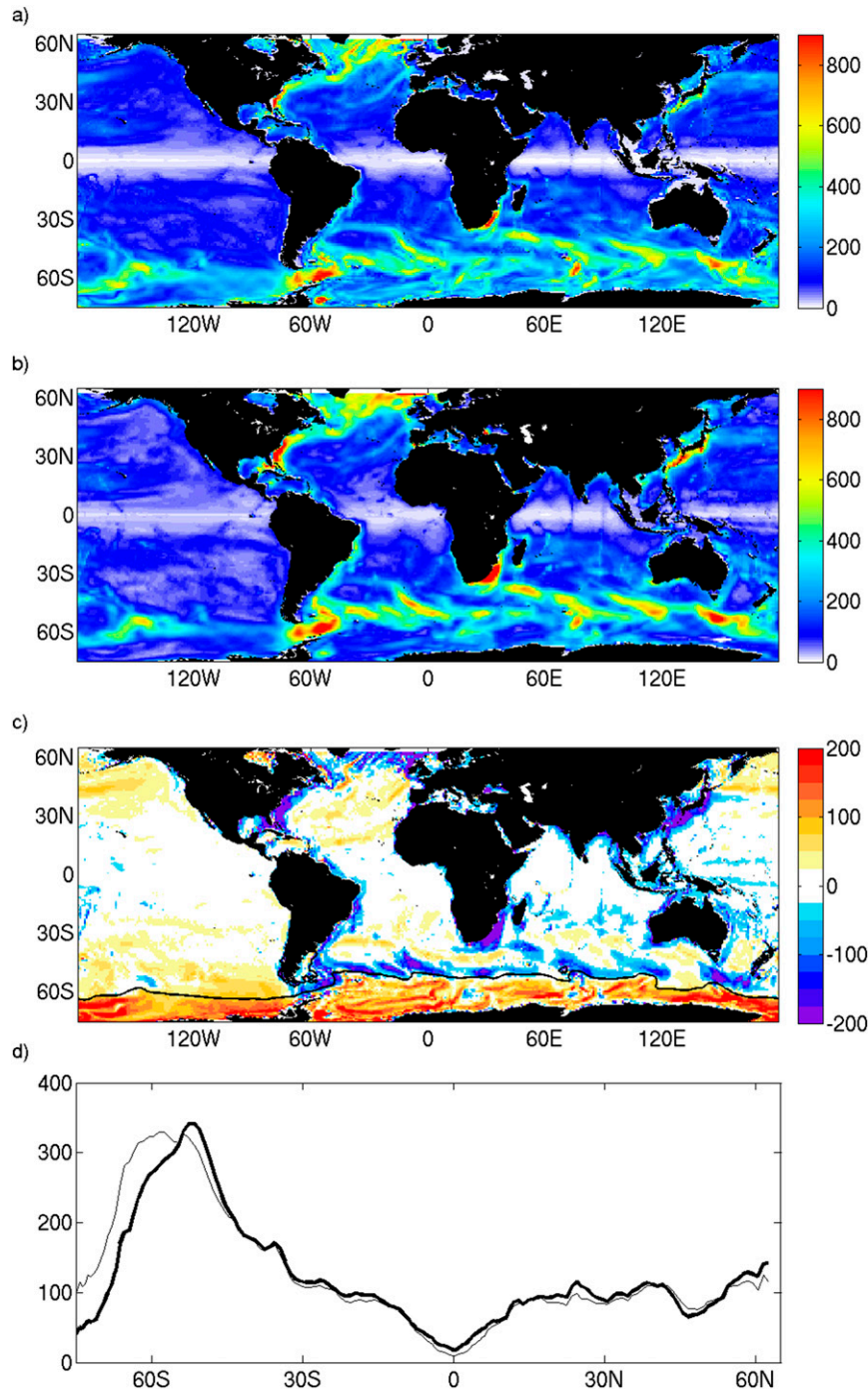


FIG. 2. Interface height diffusivities (in  $\text{m}^2 \text{s}^{-1}$ ) for year 1863 (a) used in the simulation and (b) diagnosed from the MEKE scheme, and (c) differences between the two [(a) minus (b)]. The dotted line in (c) shows the position of the polar front. (d) Zonal mean of the interface height diffusivities (in  $\text{m}^2 \text{s}^{-1}$ ) used in the simulation (thin line) and diagnosed from the MEKE scheme (thick line) for year 1863 in the pi-control simulation.

interface height diffusivities that are inferred from MEKE are compared to the interface height diffusivities that are actually used in the simulation. Differences between the interface height diffusivities diagnosed

from MEKE and those used in the model are expected since the two schemes do not rely on the same hypothesis, but overall the pattern and amplitude of the interface height diffusivities should be consistent.

The interface height diffusivity inferred from the MEKE scheme equilibrates within 2 years after initializing MEKE with zero energy. Therefore, results are shown for year 1863 (Fig. 2). Overall, a good agreement in the interface height diffusivities is found. Interface height diffusivities are maximum in the Southern Ocean, where the wind power input is large and eddies are vigorous and ubiquitous. However, the maximum interface height diffusivities occurring in the Southern Ocean inferred from the MEKE scheme are shifted equatorward compared to the maximum interface height diffusivities occurring in the Southern Ocean in the simulation (Fig. 2d).

The spatial distribution of the vertically averaged thickness diffusivities is well captured with the MEKE scheme (cf. Figs. 2a,b), although the MEKE scheme gives stronger interface height diffusivities in coastal regions and western boundary currents, and weaker interface height diffusivities at high latitudes. In the Southern Ocean, the patches of strong eddy kinetic energy (corresponding to strong values of interface height diffusivities) are even stronger in the MEKE diagnostic, but the MEKE interface height diffusivities are weaker than the ones used in the model poleward of the polar front [determined here as the position of the 2°C isotherm at 200-m depth in the Southern Ocean following Orsi et al. (1995)], which roughly delimits the poleward extension of the Antarctic Circumpolar Current.

The overall agreement in terms of amplitude and spatial patterns of the interface height diffusivities used in the simulation and diagnosed from the MEKE scheme indicates that the MEKE scheme predicts a mesoscale eddy kinetic energy that is consistent (in terms of amplitude and large-scale distribution) with the ocean state in the simulation.

The resolved bottom velocities are generally higher than the parameterized bottom mesoscale velocities (cf. Figs. 3a,b). The 2000–08 mean total bottom speed (due to both resolved and unresolved bottom velocities) of the historical simulation (Fig. 3c) is compared to bottom velocities of a  $1/8^\circ$  simulation of GOLD under present climate conditions [the same simulation that was used by Nikurashin and Ferrari (2011) in their estimate of the energy flux into lee waves]. The spatial distribution of the bottom speed is overall consistent, with the highest bottom speed found in the Southern Ocean. Differences are mainly found in the equatorial band, where the bottom speed is due to deep zonal jets that are not resolved or parameterized in the coarse-resolution GOLD model, in the Agulhas Leakage because of the absence of Agulhas eddies (which are not resolved or parameterized in the coarse-resolution GOLD model) and in

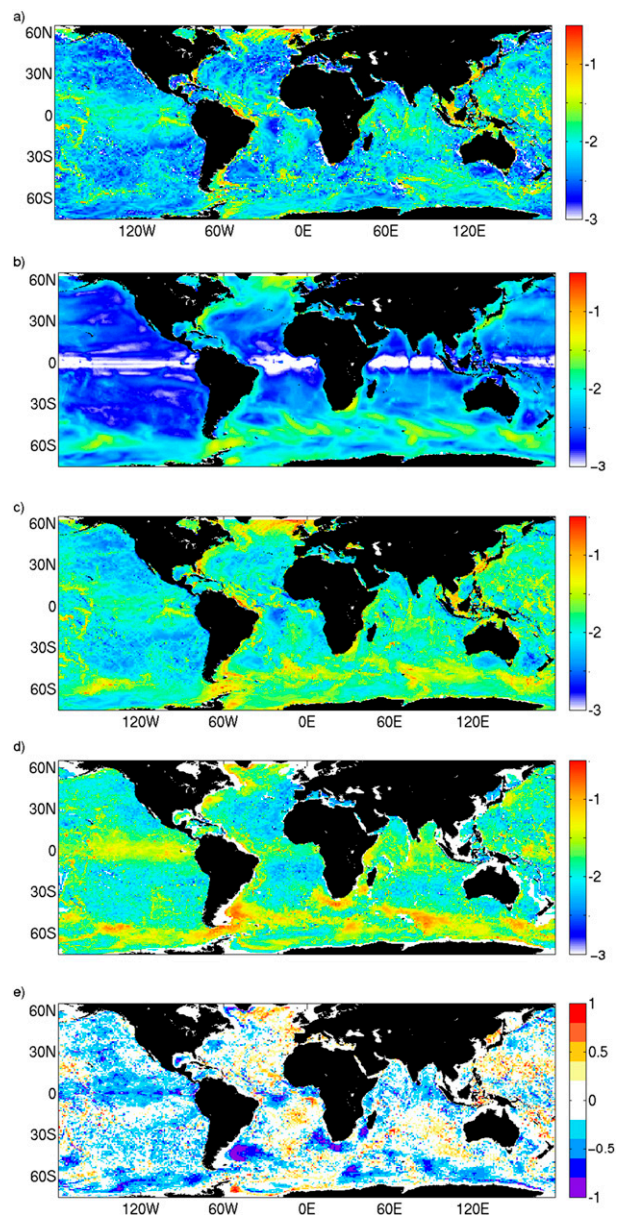


FIG. 3. Historical simulation 2000–08 mean (computed from monthly outputs) of (a) the resolved bottom speed, (b) the parameterized mesoscale bottom speed, and (c) total bottom speed [sum of (a) and (b)] in  $\log_{10}$  scale (in  $\text{m s}^{-1}$ ). (d) Bottom speed in a  $1/8^\circ$  GOLD simulation, in  $\log_{10}$  scale (in  $\text{m s}^{-1}$ ). (e)  $\log_{10}$  of the ratio of the climate model historical 2000–08 mean bottom speed (c) over the  $1/8^\circ$  GOLD simulation bottom speed (d).

the Zapiola anticyclone region. The bottom speed also tends to be weaker in the Southern Ocean in the coarse-resolution GOLD model.

Based on this analysis, it is reasonable to suggest that CM2G simulates bottom velocities and stratification adequately well for this exploratory sensitivity study.

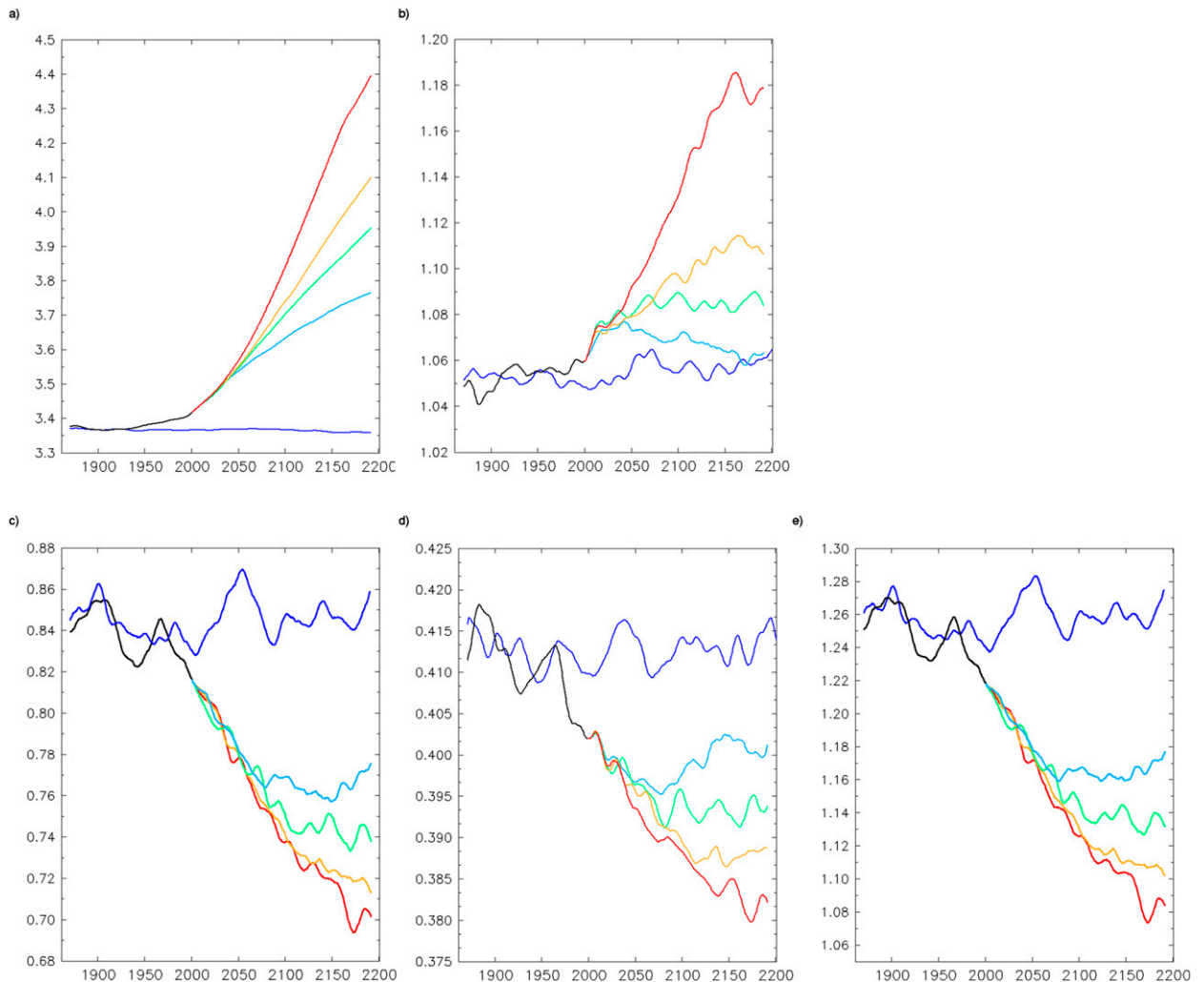


FIG. 4. Time series of the global mean (a) ocean temperature (in  $^{\circ}\text{C}$ ), (b) bottom stratification (multiplied by  $10^3$ , in  $\text{s}^{-1}$ ), (c) resolved bottom speed (in  $\text{cm s}^{-1}$ ), (d) parameterized mesoscale bottom speed (in  $\text{cm s}^{-1}$ ), and (e) total bottom speed [sum of (c) and (d), in  $\text{cm s}^{-1}$ ] for the pi-control (in dark blue), historical (in black), RCP2.6 (in light blue), RCP4.5 (in green), RCP6.0 (in orange), and RCP8.5 (in red) simulations. A low-pass filter (Sparzen filter with a window of 19 yr) has been applied to the time series.

### 3. Results

#### a. Evolution of the energy flux into lee waves from preindustrial to present and future climates

Before analyzing the evolution of the rate of conversion of the energy flux into lee waves from 1861 to 2200, we first look at the evolution of the bottom stratification and bottom velocity since these variables directly impact the conversion rate (9). Figure 4 shows the time series of the global mean ocean temperature, bottom stratification, resolved bottom velocity, parameterized bottom mesoscale velocity, and total bottom velocity. The warming of the ocean (Fig. 4a) induces an increase of the bottom stratification from 1861 to 2200 over the historical period and under the different RCP scenarios

(Fig. 4b). By contrast, both the resolved and parameterized mesoscale bottom velocities decrease over time (Figs. 4c,d). Globally, the resolved bottom velocities explain  $\frac{2}{3}$  of the total bottom velocities (Fig. 4e), with the parameterized bottom mesoscale velocity explaining the remaining  $\frac{1}{3}$ . The weakening of the global total bottom velocity from 1861 to 2200 in the historical/RCP simulations is largely ( $\sim 80\%$ ) explained by the weakening of the resolved bottom velocity.

The calculations of the energy flux into lee waves were performed in this section using the linear theory [(9)], with monthly means of model outputs, and were then averaged to give an annual mean energy flux. Time series of the global integral of the energy flux into lee waves are presented in Fig. 5a. The global energy flux

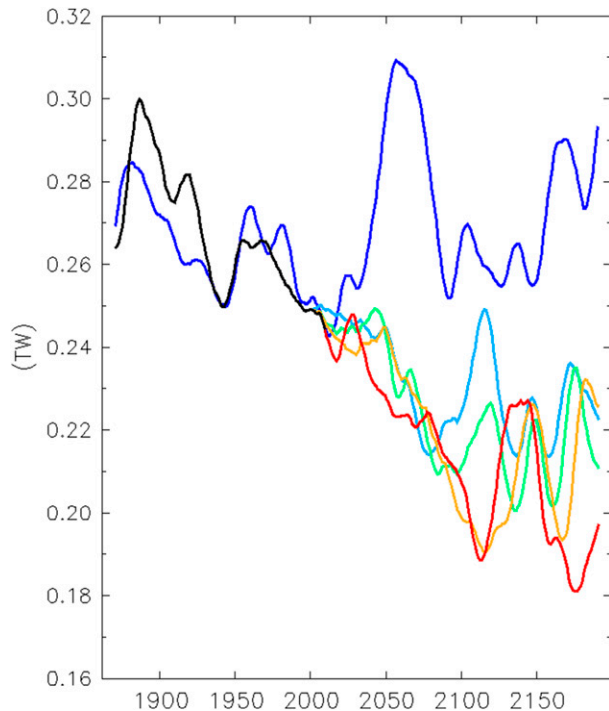


FIG. 5. (a) Time series of the global energy flux into lee waves (in TW) computed from the linear theory for the pi-control (in dark blue), historical (in black), RCP2.6 (in light blue), RCP4.5 (in green), RCP6.0 (in orange), and RCP8.5 (in red) simulations. A low-pass filter (Sparzen filter with a window of 19 yr) has been applied to the time series.

into lee waves for the preindustrial and present climates is in the range 0.24–0.32 TW for both the pi-control and historical simulations. These values are consistent with the estimate of 0.2–0.4 TW given by Nikurashin and Ferrari (2011) and Scott et al. (2011) for the present climate, but are lower than the estimate of Wright et al. (2014).

The amplitudes of the global energy fluxes into lee waves inferred from the pi-control and historical simulations are consistent before year 2000. However, large interannual and decadal variabilities are found in both simulations. In the pi-control experiment, this variability is only due to the natural variability of the climate system and therefore gives an estimate of the natural variability of the global energy flux into lee waves.

Over the twenty-first and twenty-second centuries, the global energy flux into lee waves weakens significantly in the simulations using the different RCP scenarios, reaching values of 0.18–0.25 TW, whereas it remains in the 0.24–0.32-TW range in the pi-control experiment. Compared to the pi-control simulation, the twenty-second-century global energy flux into lee waves is 26% weaker in the RCP8.5 simulation, 23% weaker in the RCP6.0 simulation, 21% weaker in the RCP4.5 simulation, and 17% weaker in the RCP2.6 simulation.

In the simulations using the historical/RCP scenarios, the decrease of the energy flux can be due to both natural variability and the changes in atmospheric forcing due to anthropogenic activities. Nevertheless, the global energy flux into lee waves consistently decreases in the RCP simulations over time, reaching low values that were not found in the pi-control run. This argues for a signature of the anthropogenic forcing on the energy flux into lee waves over the twenty-first and twenty-second centuries.

Hovmöller diagrams of the zonal average of the anomalies of the energy flux into lee waves from the 1981–2000 period as a function of time show that indeed, at most latitudes, the energy flux into lee waves tends to decrease over time in the historical/RCP8.5 simulation whereas it fluctuates with no clear long-term trend in the pi-control run (Figs. 6a,b). An exception is found in the 50°–60°S band where the energy flux into lee waves increases over time in the historical/RCP8.5 simulation.

Changes in the energy flux into lee waves computed from the linear theory are related to changes in the resolved bottom velocity and to changes in hydrography. Changes in hydrography are due to both changes in the bottom stratification and available potential energy translated through MEKE to changes in bottom kinetic energy. Hovmöller diagrams of the zonal average of anomalies of resolved bottom speed, mesoscale bottom speed, and bottom buoyancy frequency are shown in Fig. 6 for both the pi-control and historical/RCP8.5 simulations. In the pi-control simulation, no clear long-term trend of these variables can be seen. In the historical/RCP8.5 simulation, both the resolved and mesoscale bottom speed decrease over time while the bottom stratification increases (with an exception over the 30°–50°S band). These changes have opposite impacts on the energy flux into lee waves. However, it should be kept in mind that the changes in bottom mesoscale velocity in MEKE are only related to changes in hydrography with no representation of the eddy compensation/saturation mechanisms (Hallberg and Gnanadesikan 2006; Morrison and Hogg 2013). Changes in MEKE are mostly due to changes in the source term, which themselves are primarily related to changes in stratification and baroclinicity. However, tracking which process is responsible for changes in the amplitude and distribution of available potential energy is difficult. Indeed, both changes in the wind field and thermal structure of the Southern Ocean would impact the available potential energy, but these different processes are interlinked. In the Southern Ocean, changes in bottom stratification and velocity might be related to the weakening of the abyssal MOC (Fig. 7) and to the poleward shift of the Antarctic Circumpolar Current, as illustrated in Fig. 8 by the positions of the polar front [determined here as the

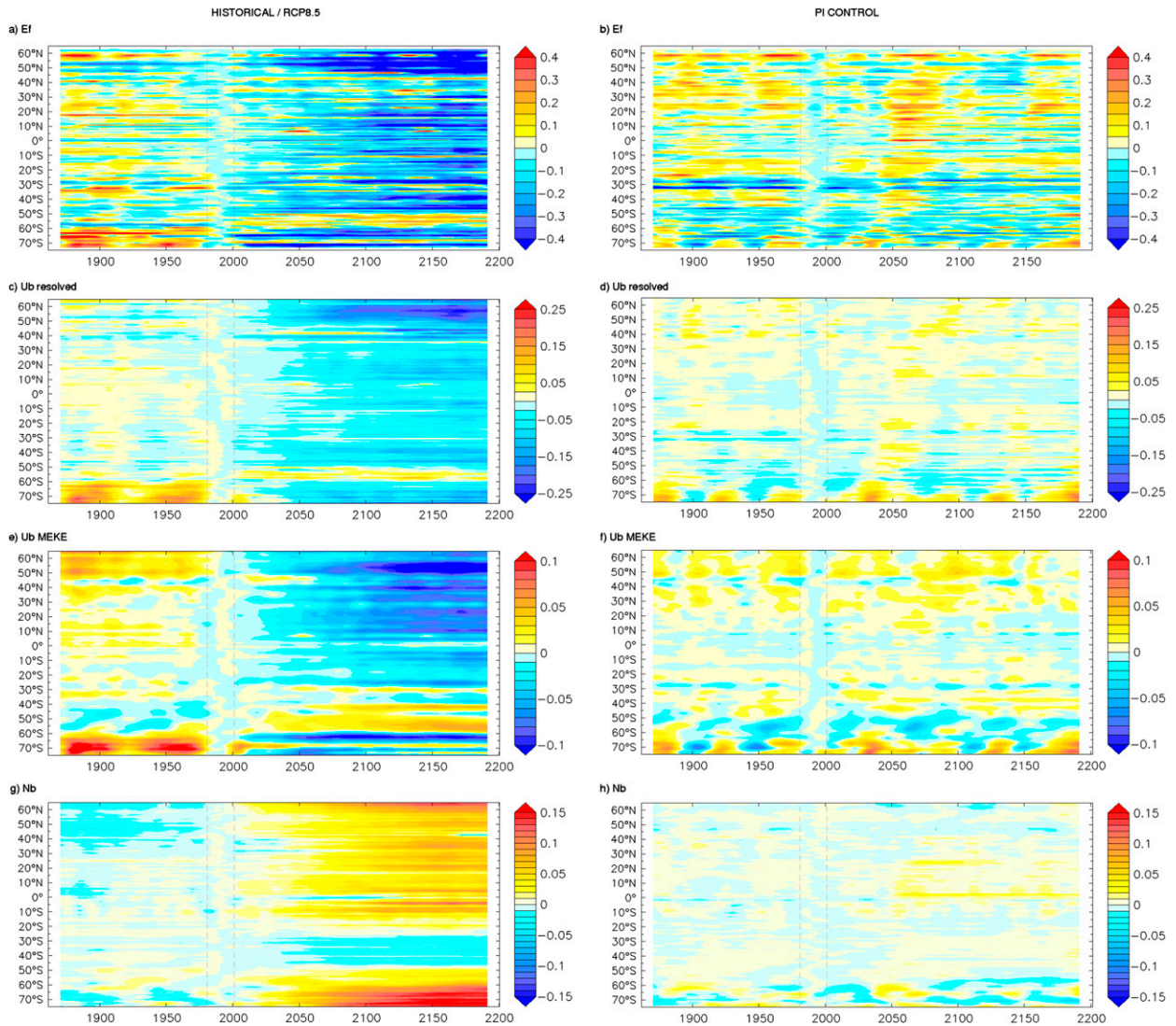


FIG. 6. Hovmöller (latitude–time) diagram of (top) the anomalies of the energy flux into lee waves (in log scale;  $\text{W m}^{-2}$ ), (middle top) the anomalies of the resolved bottom speed (in log scale,  $\text{cm s}^{-1}$ ), (middle bottom) the anomalies of the MEKE bottom speed (in log scale,  $\text{cm s}^{-1}$ ), and (bottom) the anomalies of the bottom stratification (in log scale,  $\text{s}^{-1}$ ). Anomalies were computed from the zonal mean of the 2D spatial mean of years 1981–2000 (representative of the present climate state). The left column corresponds to the historical/RCP8.5 simulation and the right column to the preindustrial control simulation. The energy flux has been computed using the linear theory and has been zonally averaged (not integrated). A low-pass filter (Sparzen filter with a window of 19 yr) has been applied in each panel. Note the different color bars.

position of the  $2^{\circ}\text{C}$  isotherm at 200-m depth following Orsi et al. (1995)] and subtropical front [determined here as the position of the  $10^{\circ}\text{C}$  isotherm at 150-m depth following Orsi et al. (1995)]. The poleward shift of the ACC is found in most climate models projections in response to the changes of the subtropical and subpolar gyres extents, and to increased transport through Drake Passage (Meehl et al. 2007; Meijers et al. 2012).

To investigate the importance of changes in bottom stratification, resolved bottom velocity and parameterized mesoscale bottom velocity in explaining the

decrease of the global energy flux into lee waves in a warmer climate, the energy flux into lee waves has been computed using a constant annual cycle (corresponding to the period 1861–80) separately for each of bottom stratification, resolved bottom velocity, and parameterized mesoscale bottom velocity for the historical/RCP6.0 simulation while other quantities evolve as before. Figure 9 shows that when a constant annual cycle is used for the bottom stratification or parameterized mesoscale bottom velocity, the global energy flux into lee waves still decreases over time at a rate comparable

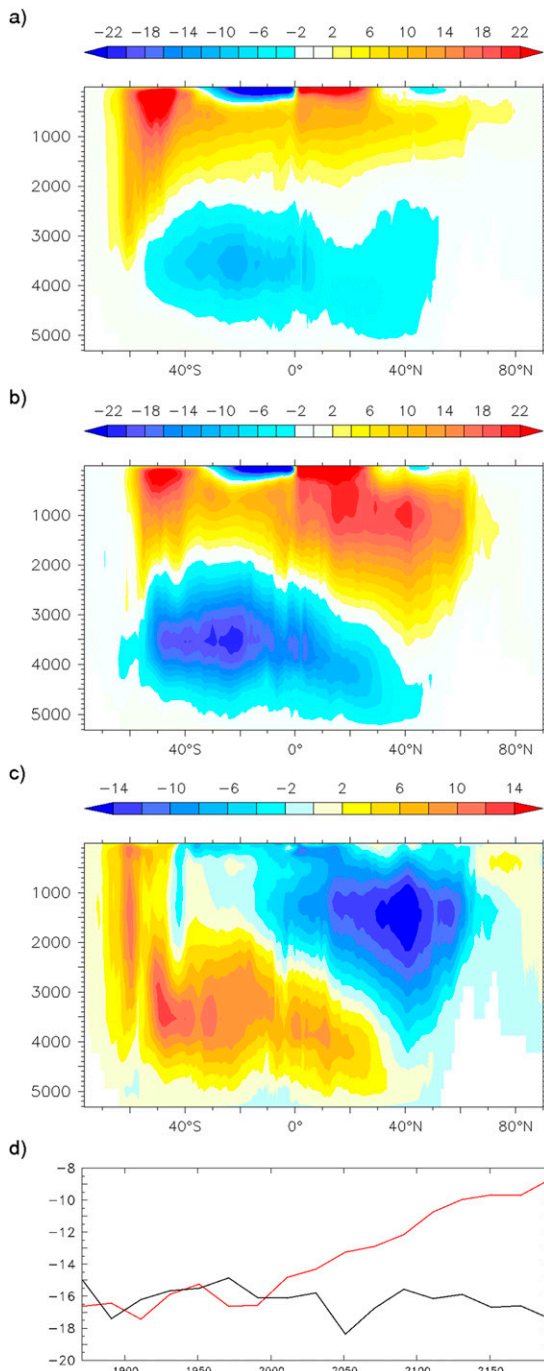


FIG. 7. Meridional overturning circulation [MOC; in Sv ( $1 \text{ Sv} \equiv 10^6 \text{ m}^3 \text{ s}^{-1}$ )] for years 2181–2200 of (a) the RCP8.5 and (b) the pi-control simulations. (c) Differences between the MOC of the RCP8.5 and pi-control simulations [(a) minus (b)]. (d) Time series (from 20-yr means) of the MOC (in Sv) averaged between 40°S and 0° and 3000–4000-m depth for the RCP8.5 (in red) and pi-control (in black) simulations.

to that of the energy flux computed from time-varying bottom stratification or parameterized mesoscale bottom velocity (cf. the yellow line and the light blue line with the black line in Fig. 9). However, when a constant annual cycle is used for the resolved bottom velocity, the global energy flux into lee waves does not show a clear long-term trend. This suggests that the decrease of the energy flux into lee waves in a warmer climate is mostly explained by the decrease of the resolved bottom velocity. This is consistent with previous results on the sensitivity of the lee wave energy flux on the bottom velocity and stratification (Trossman et al. 2013; Wright et al. 2014). Note that in Fig. 9, the global energy flux computed with a constant annual cycle for the resolved bottom velocity is weaker than the global energy flux computed with a time-varying resolved bottom velocity even in the 1861–80 period. This can be attributed to the smoothing effect on the resolved bottom velocity of using a 20-yr mean annual cycle, leading to less energetic bottom currents.

Maps of the energy flux into lee waves, resolved bottom speed, diagnosed mesoscale eddy bottom speed, and bottom stratification for the pi-control and RCP8.5 simulations as well as their differences are respectively shown in Figs. 10–13 for the twenty-second-century mean (to smooth out the impact of natural variability). Regions experiencing high rates of energy conversion from the geostrophic flows into lee waves demonstrate the greatest decrease of the energy flux in the RCP8.5 scenario compared to the pi-control simulation (Fig. 10). Yet, patches of significant increase of the energy flux are found in the Southern Ocean. Changes in the energy flux in the Southern Ocean seem to be mostly related to changes in both the resolved bottom speed (cf. Figs. 10c and 11c) and the mesoscale eddy bottom speed (cf. Figs. 10c and 12c). This is consistent with Fig. 6 and with a strengthening ACC and associated mesoscale activity. The increase in bottom stratification in the Southern Ocean might also play a role, but likely of less importance than changes in bottom speed. Outside the Southern Ocean, changes in the energy flux are mostly related to changes in the bottom resolved speed (together with changes in the mesoscale eddy bottom speed changes in the northeastern Atlantic; Fig. 12c).

While the Southern Ocean (south of 30°S) accounts for a large fraction of the global energy flux into lee waves ( $\sim 35\%$  in Figs. 10a,b), and for a large fraction of its changes in a warmer climate (20%; Fig. 10c), no clear long-term trend of the energy flux into lee waves integrated over the Southern Ocean (south of 30°S) is seen in our study (not shown). This is explained by compensation effects (decrease of the energy flux over most latitudes of the Southern Ocean under the RCP8.5 scenario (Fig. 6), but increase in the 50°–60°S band).

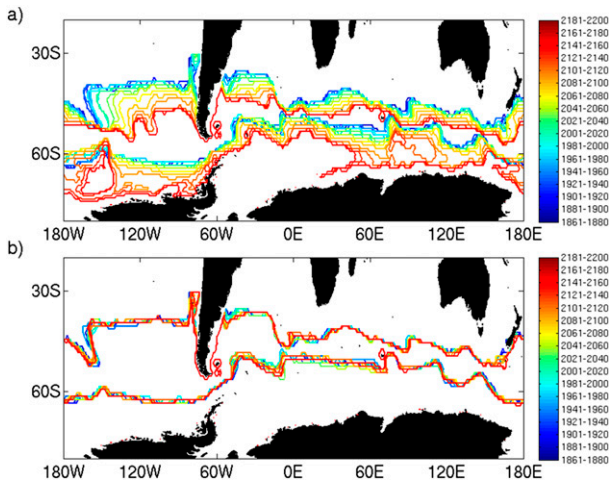


FIG. 8. Positions of the polar and subtropical fronts from 1861 to 2200 using 20-yr means in (a) the historical/RCP8.5 simulation and (b) the pi-control simulation.

#### b. Annual cycle of the energy flux into lee waves in the Southern Ocean

South of 30°S, a clear annual cycle of the energy flux into lee waves is simulated with a maximum in August–September and a minimum in January–March (Fig. 14a). To investigate the origin of the annual cycle of the energy flux into lee waves in the Southern Ocean, we first look at the annual cycle in the Southern Ocean of the different physical variables that directly impact the conversion rate (9): the bottom stratification, parameterized mesoscale bottom velocity, resolved bottom velocity, and total bottom velocity. Figure 14c shows that both the bottom stratification (yellow line) and the resolved bottom velocity (purple line) exhibit an annual cycle that is phased with the annual cycle of the energy flux into lee waves, with maxima in August–October and minima in January–March. The energy flux into lee waves also depends on the bottom stratification and speed via the steepness parameter used for correction at supercritical slopes and via the range of topographic wavenumbers leading to propagating lee waves. To further examine the impact of the annual cycle of the bottom stratification and speed on the annual cycle of the energy flux into lee waves, the same methodology as used for explaining the long-term decrease of the global energy flux (Fig. 9) is used. The energy flux into lee waves is first computed in the pi-control simulation using years 1861–2200 mean annual cycle for the bottom stratification and velocities (black line in Fig. 14b). The corresponding annual cycle of the energy flux presents the same phasing as the annual cycle of the energy flux into lee waves computed from monthly means over the 1861–2200 period (Fig. 14a, black line). Then, the energy

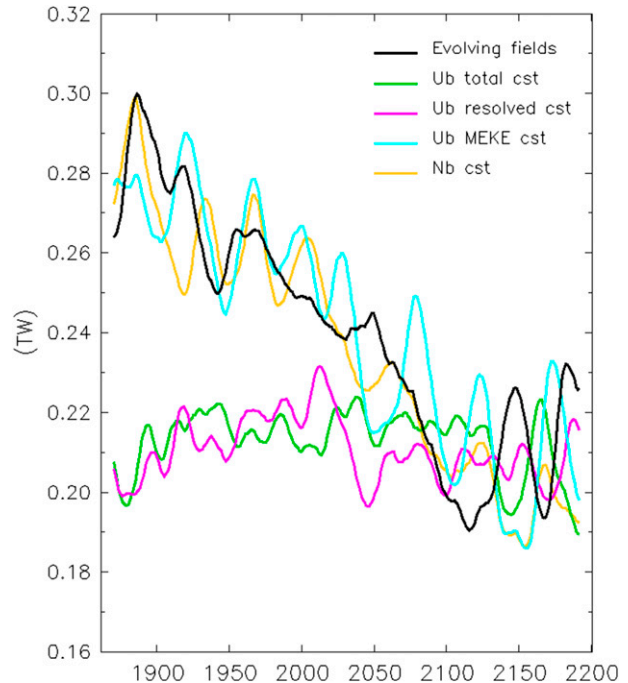


FIG. 9. Time series of the global energy flux into lee waves (in TW) for the historical/RCP6 scenario simulation computed from the linear theory (black line; same curve as the orange curve in Fig. 5a) and using a constant mean 1861–80 annual cycle for the bottom speed (green line), the bottom unresolved speed (MEKE, light blue line), the bottom resolved speed (purple line), and the bottom stratification (yellow line).

flux into lee waves is computed using the years 1861–2200 mean value of one quantity (bottom stratification, parameterized mesoscale bottom velocity, resolved bottom velocity, or total bottom velocity) while using the 1861–2200 mean annual cycle for the other quantities. Figure 14b shows that when a constant value is used for the parameterized mesoscale bottom velocity or the bottom stratification, the annual cycle of the energy flux into lee waves is still comparable to that of the energy flux computed from the annual cycles of all physical quantities (cf. the yellow line and the light blue line with the black line in Fig. 14b). However, when the resolved bottom velocity is held at its 1861–2200 mean value, the energy flux into lee waves in the Southern Ocean shows a much weaker annual cycle with a maximum in December–January and a minimum in May. The same result is obtained when the total bottom velocity is held at its 1861–2200 mean value. This suggests that the annual cycle of the energy flux into lee waves in the Southern Ocean is mostly explained by the annual cycle of the resolved bottom velocity.

#### 4. Conclusions and discussions

Internal lee waves are generated by the interaction of geostrophic flows with rough topography in the stratified

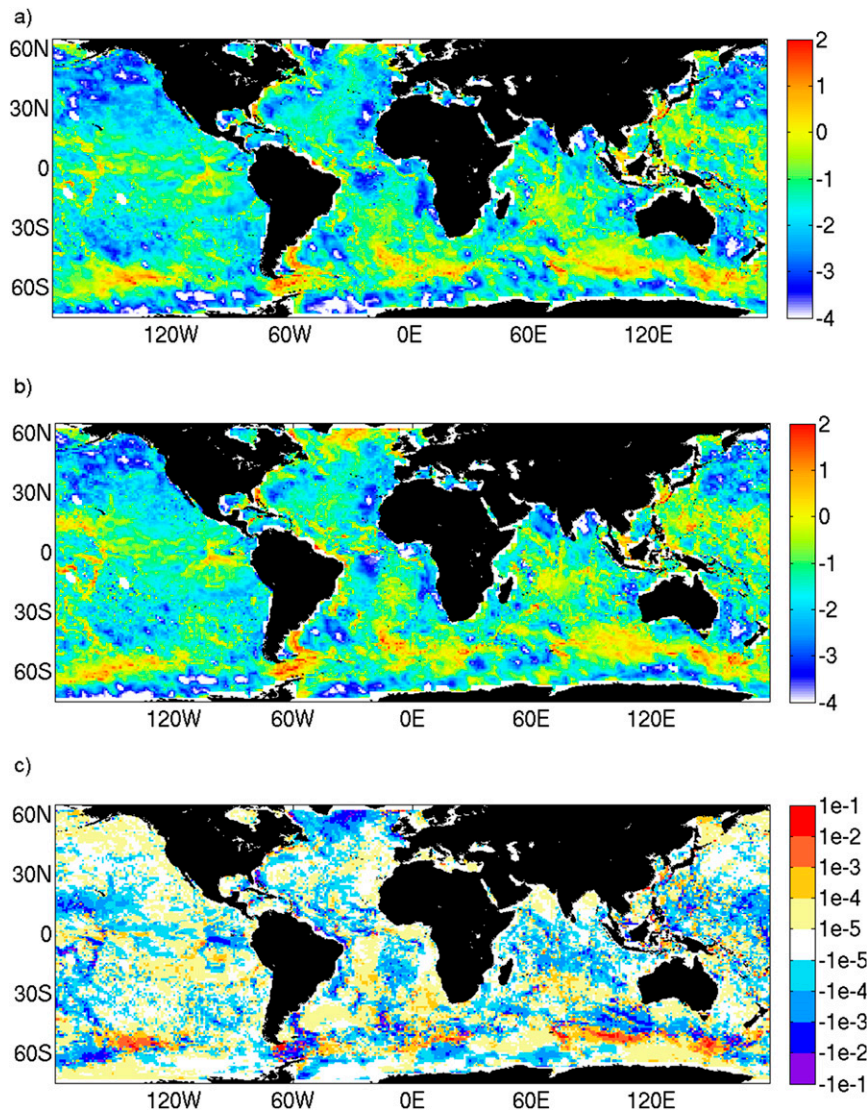


FIG. 10. Twenty-second-century mean of the energy flux into lee waves using the linear theory with (a) the RCP8.5 simulation (in  $\log_{10}$  scale, units in  $\text{mW m}^{-2}$ ) and (b) the pi-control simulation (in  $\log_{10}$  scale, units in  $\text{mW m}^{-2}$ ). (c) Difference between (a) and (b) (in  $\text{W m}^{-2}$ ).

ocean. Their breaking is thought to play a significant role for the dissipation of eddy energy in the ocean and for sustaining diapycnal mixing in the deep ocean, and therefore for the maintenance of the deep ocean stratification and global overturning circulation. Thus, lee-wave-driven mixing warrants serious consideration, and is becoming an area of active research. A key ingredient for understanding and constraining lee-wave-driven mixing is the energy flux that is transferred from geostrophic flows into lee waves. Two recent estimates of the energy flux into lee waves have been computed by Nikurashin and Ferrari (2011) and Scott et al. (2011) based on the linear wave theory of Bell (1975). The static estimate by Nikurashin and Ferrari (2011) was used in

Melet et al. (2014) to parameterize lee-wave-driven mixing in a climate model. While Melet et al. (2014) show that lee-wave-driven mixing makes a significant impact on the ocean state and should be specifically parameterized in ocean models, they argue that the energy flux into lee waves used in the parameterization should depend on the ocean state to allow the internal lee-wave-driven mixing to evolve in a changing ocean.

In the present study, we aimed at exploring the evolution of the energy flux into lee waves from preindustrial to possible future climate conditions. To do so, we used the linear wave theory developed in Nikurashin and Ferrari (2011) and applied it from year 1861 to year 2200. The bottom stratification and velocity used for the calculation

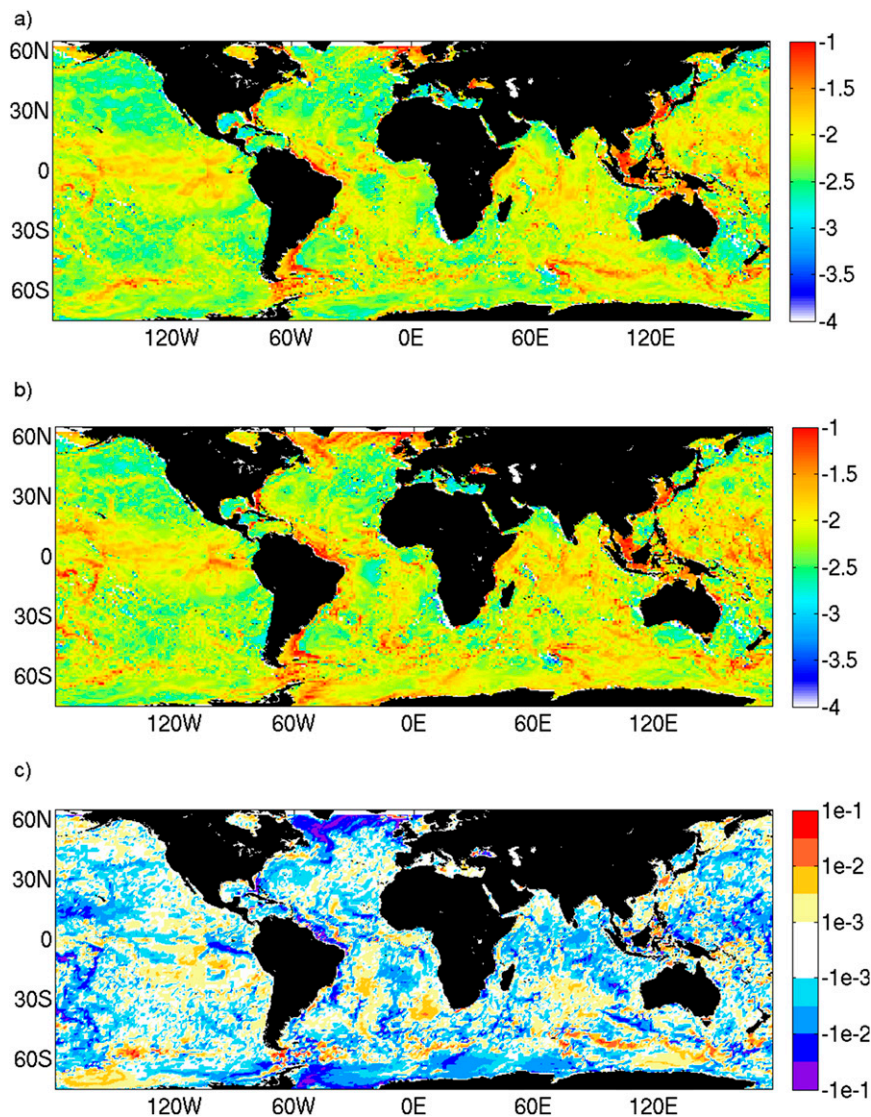


FIG. 11. Twenty-second-century mean of the resolved bottom speed in (a) the RCP8.5 simulation (in  $\log_{10}$  scale) and (b) the pi-control simulation (in  $\log_{10}$  scale). (c) Difference between (a) and (b). Units are in  $\text{m s}^{-1}$ .

are simulated from the GFDL CM2G climate model used for the IPCC AR5 suite using historical forcing and RCP2.6, RCP4.5, RCP6.0, and RCP8.5 scenarios. The mesoscale eddy velocity, unresolved in the climate model, is parameterized based on a 2D equation for the evolution of the mesoscale eddy energy (MEKE) following the ideas of [Eden and Greatbatch \(2008\)](#) and [Marshall and Adcroft \(2010\)](#). The parameterization of the mesoscale eddy energy (referred to as the MEKE scheme) captures both the patterns and rough magnitude of mesoscale eddy energy induced from the same ocean model run at a higher resolution and used in the estimate of the energy flux into lee waves by [Nikurashin and Ferrari \(2011\)](#). The interface height diffusivities

passively diagnosed from the MEKE scheme also compare well with the interface height diffusivities that are actually used in the simulation. Therefore, the MEKE scheme can be used as a passive diagnostic to parameterize the bottom mesoscale eddy energy and velocity. Using the climate model to infer the ocean bottom stratification, resolved velocity, and mesoscale eddy velocity, the evolution of the energy flux into lee waves is computed based on the linear theory for both a control simulation in which the forcing due to aerosols and other radiatively active gases is held at preindustrial levels. The same is accomplished for simulations using the historical concentrations of aerosols and other radiatively active gases and the RCP scenarios. We show that the energy

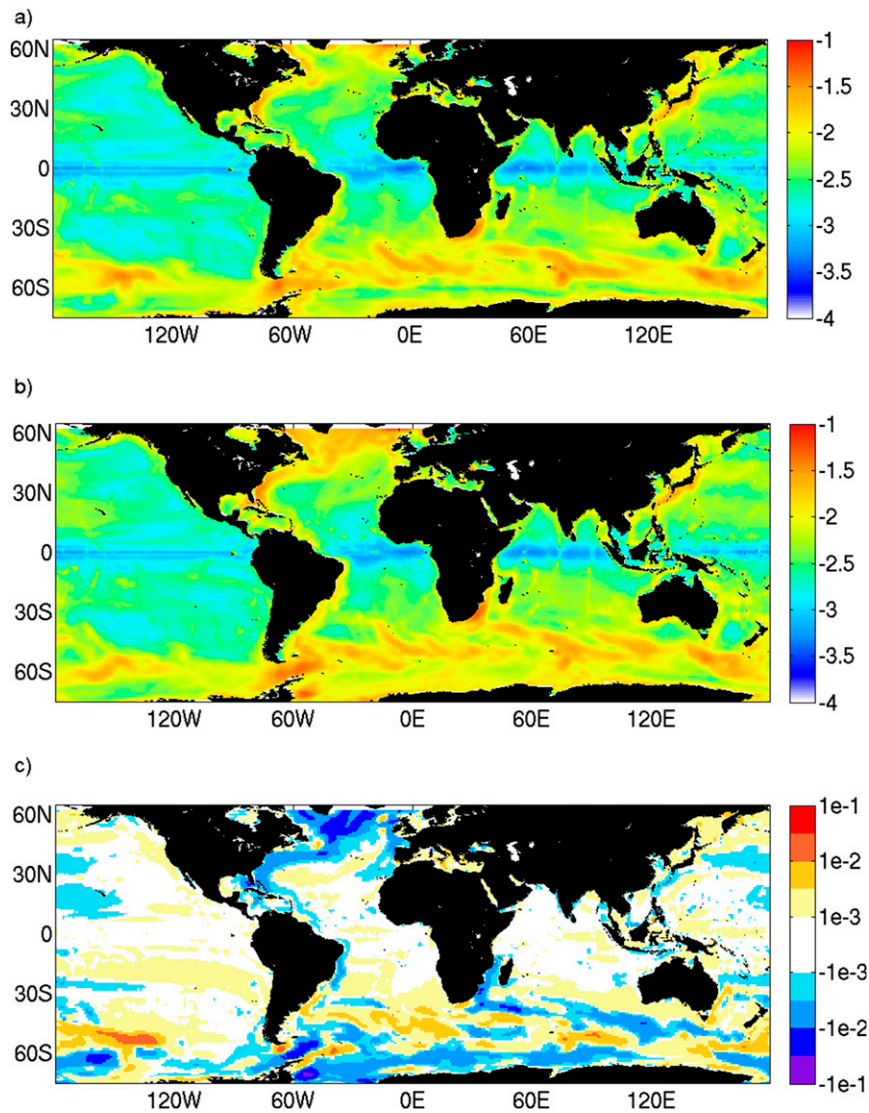


FIG. 12. As in Fig. 11, but for MEKE bottom speed.

flux into lee wave significantly evolves in time, with a long-term decrease of the global energy flux into lee waves over the next two centuries in the historical/RCP simulations. The energy flux into lee waves also exhibits a clear annual cycle in the Southern Ocean, reaching its maximum in austral winter. The annual cycle is mostly explained by the annual cycle of the bottom velocities, the ACC and related eddy activity being strong in austral winter. The time variability of the energy flux into lee waves suggested in the present study when the energy flux is impacted by changes in winds, bottom speed, and stratification warrants the use of a state-dependent, time-evolving energy flux in lee-wave-driven mixing parameterization in climate models.

Our estimates of lee wave energy flux rely on existing linear lee wave theory calculations and datasets which

are subject to different uncertainties. Regarding the linear wave theory, topographic blocking and splitting effects have been shown to impact the energy flux into lee waves (Nikurashin et al. 2014). The correction we used in this study for the saturation of the energy flux into lee waves at supercritical slopes is the same as in previous lee wave radiation estimates (e.g., Nikurashin and Ferrari 2011; Scott et al. 2011) and therefore uses a critical steepness parameter of 0.7. While this value is based on studies using 2D topographies, smaller critical steepness parameter (of  $\sim 0.4$ ) should be used for 3D topographies (Nikurashin et al. 2014). Saturation at a smaller critical steepness parameter is due to 3D splitting and blocking effects and leads to better agreement with observations (e.g., St. Laurent et al. 2012; Waterman et al. 2013; Sheen et al.

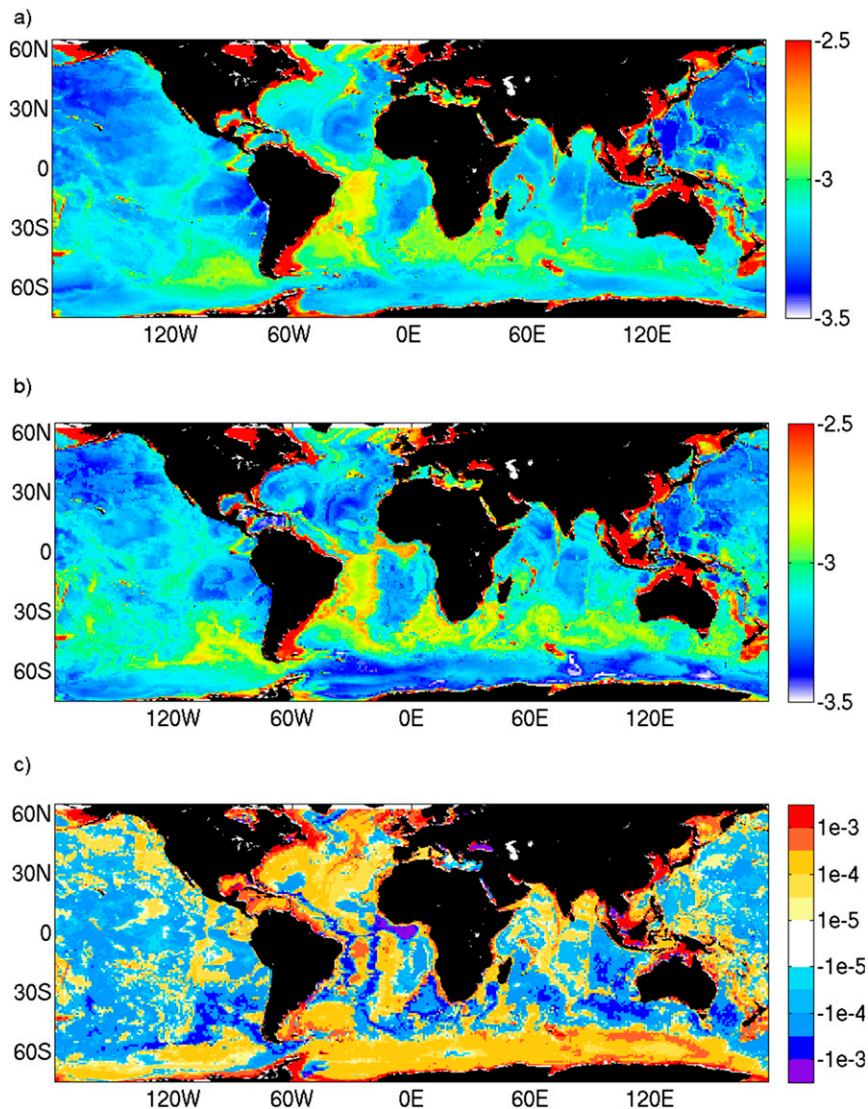


FIG. 13. As in Fig. 11, but for bottom stratification.

2013). The topographic spectra used in this study for estimating the energy flux into lee waves are isotropic and have a coarse spatial resolution. While abyssal hill anisotropy is expected to impact regional lee wave radiation estimates, it is not expected to strongly impact the global integral of the energy flux into lee waves. Given the consistency of the estimates of the energy flux into lee waves of Nikurashin and Ferrari (2011) and Scott et al. (2011) based on three independent topographic products [isotropic topographic spectrum based on single beam acoustic data in Nikurashin and Ferrari (2011), topographic spectrum based on paleo-spreading rates (Goff and Arbic 2010), and small-scale altimeter-derived gravity roughness (Goff 2010) in Scott et al. (2011)], we conclude that uncertainties in the topographic

spectrum used in this study should not strongly impact our conclusions on the evolution of the energy flux into lee waves under possible future climate conditions. Because of these different assumptions made in the linear wave theory estimate of the energy flux, our results are not expected to be accurate locally. However, this study does not aim to improve existing linear wave theory calculations but rather to use them to study the sensitivity of lee wave radiation to changes in climate conditions.

The bottom stratification and velocity used in our calculations of the energy flux under changing climates are simulated by the CM2G climate model and are also subject to uncertainties. Regarding the bottom velocities, our results rely on both the resolved and parameterized mesoscale eddy bottom velocities. It should be

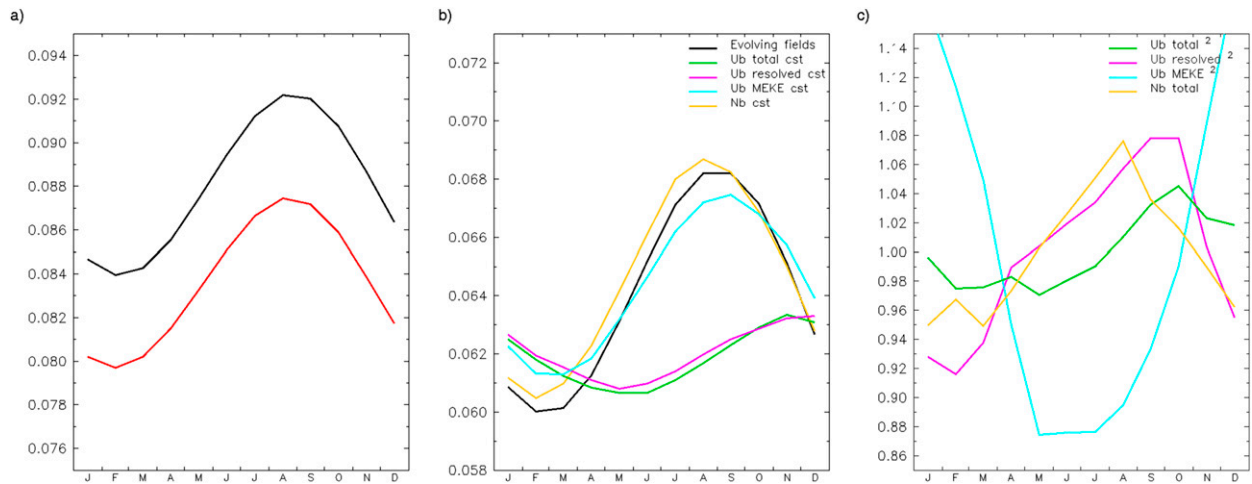


FIG. 14. (a) Annual cycle of the energy flux into lee waves integrated over the Southern Ocean (south of 30°S; in TW) for the pi-control (in black) and historical simulation/RCP8.5 projection (in red) over the 1861–2200 period. (b) Annual cycle of the energy flux into lee waves integrated over the Southern Ocean (south of 30°S; in TW) computed from the 1861–2200 mean annual cycle of the bottom stratification and speed for the pi-control (in black), and a constant 1861–2200 mean bottom speed (green line), constant 1861–2200 bottom unresolved speed (MEKE, light blue line), constant 1861–2200 bottom resolved speed (purple line), and constant 1861–2200 bottom stratification (yellow line). (c) 1861–2200 mean annual cycle of the physical variables impacting the energy flux into lee waves, divided by their 1861–2200 mean: squared bottom speed (green line), squared bottom unresolved speed (MEKE, light blue line), squared bottom resolved speed (purple line), and bottom stratification (yellow line).

clear that the MEKE eddy-induced bottom velocities are not expected to be locally accurate. The parameters used within the MEKE closure are not fundamental and were determined empirically. In particular, the ratio of bottom over vertical-mean mesoscale eddy velocity ( $\alpha$ ) is not expected to be globally uniform and constant. Furthermore, the pattern of mean energy extraction by eddies might change under a changing climate, either in amplitude or location, due to mean state changes. However, at leading order we do not expect the nature of eddy or dissipation processes to be very different. Assuming an equilibrium for the mesoscale energy cycle, the pattern or amplitude of eddy energy dissipation must respond to a change in mean flow energy extraction. These assumptions allow us to tune the MEKE parameters for contemporary climate and then apply the MEKE model with those same parameters in a changed climate. Furthermore, eddy compensation/saturation mechanisms are neglected in the estimate of the mesoscale eddy-induced bottom velocities.

Finally, Trossman et al. (2013) showed that when lee wave generation was accounted for in an ocean model through a momentum-flux-based parameterization, the modeled bottom stratification was significantly reduced while the bottom speed was also slightly reduced. Lee wave generation exerts a drag force on the geostrophic flow, acting as a sink for the mesoscale eddy energy. This feedback was neglected in this study, and would require the MEKE closure scheme to be used interactively in the

ocean model. It should also be noted that the model used in this study does not take into account the mixing associated with the dissipation of lee waves. As lee-wave-driven mixing impacts the stratification in the deep ocean (Trossman et al. 2013; Melet et al. 2014), this could lead to feedbacks on the energy flux into lee waves and the mesoscale eddy energy. Despite these different sources of uncertainties, our estimate for the present day conditions compares well with the estimates by Nikurashin and Ferrari (2011) and Scott et al. (2011), which gives some confidence in our results and their relevance to the real ocean.

Regarding the evolution of the energy flux from pre-industrial to present to twenty-second-century climate conditions, the future emissions of radiatively active gases and aerosols are other sources of uncertainty.

Despite these uncertainties, we believe that our estimates of the evolution of the energy flux into lee waves integrated over the global or Southern Ocean, showing a long-term decrease of the global energy flux under a warming climate, are qualitatively robust.

**Acknowledgments.** The authors thank Malte Jansen and John Dunne for helpful discussions and John Krasting for his help in setting up the simulations. We also thank three anonymous reviewers for thoughtful comments on this manuscript. This work is a component of the internal wave driven mixing Climate Process Team funded by the National Science Foundation Grant OCE-0968721 and the National Oceanic and Atmospheric

Administration, U.S. Department of Commerce, Award NA08OAR4320752. The statements, findings, conclusions, and recommendations are those of the authors and do not necessarily reflect the views of the National Oceanic and Atmospheric Administration, or the U.S. Department of Commerce.

## REFERENCES

- Arbic, B. K., and G. R. Flierl, 2004: Baroclinically unstable geostrophic turbulence in the limit of strong and weak bottom Ekman friction: Application to mid-ocean eddies. *J. Phys. Oceanogr.*, **34**, 2257–2273, doi:10.1175/1520-0485(2004)034<2257:BUGTIT>2.0.CO;2.
- Bates, M., R. Tulloch, J. Marshall, and R. Ferrari, 2014: Rationalizing the spatial distribution of mesoscale eddy diffusivity in terms of mixing length theory. *J. Phys. Oceanogr.*, **44**, 1523–1540, doi:10.1175/JPO-D-13-0130.1.
- Bell, T. H., 1975: Topographically generated internal waves in the open ocean. *J. Geophys. Res.*, **80**, 320–327, doi:10.1029/JC080i003p00320.
- Booth, J., and I. Kamenkovich, 2008: Isolating the role of mesoscale eddies in mixing of a passive tracer in an eddy resolving model. *J. Geophys. Res.*, **113**, C05021, doi:10.1029/2007JC004510.
- Brearley, J. A., K. L. Sheen, A. C. Naveira Garabato, D. A. Smeed, and S. Waterman, 2013: Eddy-induced modulation of turbulent dissipation over rough topography in the Southern Ocean. *J. Phys. Oceanogr.*, **43**, 2288–2308, doi:10.1175/JPO-D-12-0222.1.
- Bryan, F. O., 1987: Parameter sensitivity of primitive equation ocean general circulation models. *J. Phys. Oceanogr.*, **17**, 970–985, doi:10.1175/1520-0485(1987)017<0970:PSOPEO>2.0.CO;2.
- Cessi, P., 2008: An energetically constrained parameterization of eddy buoyancy flux. *J. Phys. Oceanogr.*, **38**, 1807–1819, doi:10.1175/2007JPO3812.1.
- Decloedt, T., and D. Luther, 2010: On a simple empirical parameterization of topography-catalyzed diapycnal mixing in the abyssal ocean. *J. Phys. Oceanogr.*, **40**, 487–508, doi:10.1175/2009JPO4275.1.
- Dunne, J. P., and Coauthors, 2012: GFDL's ESM2 global coupled climate-carbon Earth system models. Part I: Physical formulation and baseline simulation characteristics. *J. Climate*, **25**, 6646–6665, doi:10.1175/JCLI-D-11-00560.1.
- Eden, C., and R. J. Greatbatch, 2008: Towards a mesoscale eddy closure. *Ocean Modell.*, **20**, 223–239, doi:10.1016/j.ocemod.2007.09.002.
- Ferrari, R., and C. Wunsch, 2009: Ocean circulation kinetic energy: Reservoirs, sources, and sinks. *Annu. Rev. Fluid Mech.*, **41**, 253–282, doi:10.1146/annurev.fluid.40.111406.102139.
- Friedrich, T., A. Timmermann, T. Decloedt, D. S. Luther, and A. Mouchet, 2011: The effect of topography-enhanced diapycnal mixing on ocean and atmospheric circulation and marine biogeochemistry. *Ocean Modell.*, **39**, 262–274, doi:10.1016/j.ocemod.2011.04.012.
- Gent, P. R., and J. McWilliams, 1990: Isopycnal mixing in ocean circulation models. *J. Phys. Oceanogr.*, **20**, 150–155, doi:10.1175/1520-0485(1990)020<0150:IMIOC>2.0.CO;2.
- Gille, S. T., M. M. Yale, and D. T. Sandwell, 2000: Global correlation of mesoscale ocean variability with seafloor roughness from satellite altimetry. *Geophys. Res. Lett.*, **27**, 1251–1254, doi:10.1029/1999GL007003.
- Gnanadesikan, A., B. L. Samuels, and R. D. Slater, 2003: Sensitivity of water mass transformation and heat transport to subgrid-scale mixing in coarse-resolution ocean models. *Geophys. Res. Lett.*, **30**, 1967, doi:10.1029/2003GL018036.
- , J. P. Dunne, R. M. Key, K. Matsumoto, J. L. Sarmiento, R. D. Slater, and P. S. Swathi, 2004: Oceanic ventilation and biogeochemical cycling: Understanding the physical mechanisms that produce realistic distributions of tracers and productivity. *Global Biogeochem. Cycles*, **18**, GB4010, doi:10.1029/2003GB002097.
- Goff, J. A., 2010: Global prediction of abyssal hill root-mean-square heights from small-scale altimetric gravity variability. *J. Geophys. Res.*, **115**, B12104, doi:10.1029/2010JB007867.
- , and T. H. Jordan, 1988: Stochastic modeling of seafloor morphology: Inversion of sea beam data for second-order statistics. *J. Geophys. Res.*, **93** (B11), 13 589–13 608, doi:10.1029/JB093iB11p13589.
- , and B. K. Arbic, 2010: Global prediction of abyssal hill roughness statistics for use in ocean models from digital maps of paleo-spreading rate, paleo-ridge orientation, and sediment thickness. *Ocean Modell.*, **32**, 36–43, doi:10.1016/j.ocemod.2009.10.001.
- Gouretski, V. V., and K. P. Koltermann, 2004: WOCE global hydrographic climatology. Berichte des Bundesamtes für Seeschifffahrt und Hydrographie Tech. Rep. 35, 52 pp.
- Hallberg, R., 2013: Using a resolution function to regulate parameterizations of oceanic mesoscale eddy effects. *Ocean Modell.*, **72**, 92–103, doi:10.1016/j.ocemod.2013.08.007.
- , and A. Gnanadesikan, 2006: The role of eddies in determining the structure and response of the wind-driven Southern Hemisphere overturning: Results from the Modeling Eddies in the Southern Ocean (MESO) project. *J. Phys. Oceanogr.*, **36**, 2232–2252, doi:10.1175/JPO2980.1.
- , and A. Adcroft, 2009: Reconciling estimates of the free surface height in Lagrangian vertical coordinate ocean models with mode-split time stepping. *Ocean Modell.*, **29**, 15–26, doi:10.1016/j.ocemod.2009.02.008.
- Heywood, K. J., A. C. Naveira Garabato, and D. P. Stevens, 2002: High mixing rates in the abyssal Southern Ocean. *Nature*, **415**, 1011–1014, doi:10.1038/4151011a.
- Ito, T., and J. Marshall, 2008: Control of lower-limb overturning circulation in the Southern Ocean by diapycnal mixing and mesoscale eddy transfer. *J. Phys. Oceanogr.*, **38**, 2832–2845, doi:10.1175/2008JPO3878.1.
- Ivchenko, V. O., S. Danilov, and J. Schröter, 2014: Comparison of the effect of parameterized eddy fluxes of thickness and potential vorticity. *J. Phys. Oceanogr.*, **44**, 2470–2484, doi:10.1175/JPO-D-13-0267.1.
- Jayne, S. R., and L. C. St. Laurent, 2001: Parameterizing tidal dissipation over rough topography. *Geophys. Res. Lett.*, **28**, 811–814, doi:10.1029/2000GL012044.
- Kunze, E., E. Firing, J. M. Hummon, T. K. Chereskin, and A. M. Thurnherr, 2006: Global abyssal mixing inferred from lowered ADCP shear and CTD strain profiles. *J. Phys. Oceanogr.*, **36**, 1553–1576, doi:10.1175/JPO2926.1.
- MacKinnon, J. A., 2013: Mountain waves in the deep ocean. *Nature*, **501**, 321–322, doi:10.1038/501321a.
- Marshall, D. P., and A. C. Naveira Garabato, 2008: A conjecture on the role of bottom-enhanced diapycnal mixing in the parameterization of geostrophic eddies. *J. Phys. Oceanogr.*, **38**, 1607–1613, doi:10.1175/2007JPO3619.1.
- , and A. Adcroft, 2010: Parameterization of ocean eddies: Potential vorticity mixing, energetics and Arnold's first stability theorem. *Ocean Modell.*, **32**, 188–204, doi:10.1016/j.ocemod.2010.02.001.

- Meehl, G. A., and Coauthors, 2007: Global climate projections. *Climate Change 2007: The Physical Science Basis*. S. Solomon et al., Eds., Cambridge University Press, 747–845.
- Meijers, A. J. S., E. Shuckburgh, N. Bruneau, J.-B. Sallee, T. J. Bracegirdle, and Z. Wang, 2012: Representation of the Antarctic Circumpolar Current in the CMIP5 climate models and future changes under warming scenarios. *J. Geophys. Res.*, **117**, C12008, doi:10.1029/2012JC008412.
- Melet, A., R. Hallberg, S. Legg, and K. L. Polzin, 2013: Sensitivity of the ocean state to the vertical distribution of internal-tide-driven mixing. *J. Phys. Oceanogr.*, **43**, 602–615, doi:10.1175/JPO-D-12-055.1.
- , —, —, and M. Nikurashin, 2014: Sensitivity of the ocean state to lee wave–driven mixing. *J. Phys. Oceanogr.*, **44**, 900–921, doi:10.1175/JPO-D-13-072.1.
- Morrison, A. K., and A. M. Hogg, 2013: On the relationship between Southern Ocean overturning and ACC transport. *J. Phys. Oceanogr.*, **43**, 140–148, doi:10.1175/JPO-D-12-057.1.
- Naveira Garabato, A. C., K. L. Polzin, B. A. King, K. J. Heywood, and M. Visbeck, 2004: Widespread intense turbulent mixing in the Southern Ocean. *Science*, **303**, 210–213, doi:10.1126/science.1090929.
- , A. J. G. Nurser, R. B. Scott, and J. A. Goff, 2013: The impact of small-scale topography on the dynamical balance of the ocean. *J. Phys. Oceanogr.*, **43**, 647–668, doi:10.1175/JPO-D-12-056.1.
- Nikurashin, M., and R. Ferrari, 2010a: Radiation and dissipation of internal waves generated by geostrophic flows impinging on small-scale topography: Theory. *J. Phys. Oceanogr.*, **40**, 1055–1074, doi:10.1175/2009JPO4199.1.
- , and —, 2010b: Radiation and dissipation of internal waves generated by geostrophic flows impinging on small-scale topography: Application to the Southern Ocean. *J. Phys. Oceanogr.*, **40**, 2025–2042, doi:10.1175/2010JPO4315.1.
- , and —, 2011: Global energy conversion rate from geostrophic flows into internal lee waves in the deep ocean. *Geophys. Res. Lett.*, **38**, L08610, doi:10.1029/2011GL046576.
- , and —, 2013: Overturning circulation driven by breaking internal waves in the deep ocean. *Geophys. Res. Lett.*, **40**, 3133–3137, doi:10.1002/grl.50542.
- , G. Vallis, and A. Adcroft, 2013: Routes to energy dissipation for geostrophic flows in the Southern Ocean. *Nat. Geosci.*, **6**, 48–51, doi:10.1038/ngeo1657.
- , R. Ferrari, N. Grisouard, and K. Polzin, 2014: The impact of finite-amplitude bottom topography on internal wave generation in the Southern Ocean. *J. Phys. Oceanogr.*, **44**, 2938–2950, doi:10.1175/JPO-D-13-0201.1.
- Nycander, J., 2005: Generation of internal waves in the deep ocean by tides. *J. Geophys. Res.*, **110**, C10028, doi:10.1029/2004JC002487.
- Orsi, A. H., T. Whitworth, and W. D. Nowlin, 1995: On the meridional extent and fronts of the Antarctic Circumpolar Current. *Deep-Sea Res. I*, **42**, 641–673, doi:10.1016/0967-0637(95)00021-W.
- Park, Y.-G., and K. Bryan, 2000: Comparison of thermally driven circulations from a depth-coordinate model and an isopycnal-layer model. Part I: Scaling-law sensitivity to vertical diffusivity. *J. Phys. Oceanogr.*, **30**, 590–605, doi:10.1175/1520-0485(2000)030<0590:COTDCF>2.0.CO;2.
- Polzin, K. L., 2009: An abyssal recipe. *Ocean Modell.*, **30**, 298–309, doi:10.1016/j.ocemod.2009.07.006.
- , and E. Firing, 1997: Estimates of diapycnal mixing using LADCP and CTD data from 18°S. *International WOCE Newsletter*, No. 29, WOCE International Project Office, Southampton, United Kingdom, 39–42.
- Saenko, O. A., A. Sen Gupta, and P. Spence, 2012: On challenges in predicting bottom water transport in the Southern Ocean. *J. Climate*, **25**, 1349–1356, doi:10.1175/JCLI-D-11-00040.1.
- Scott, R. B., and Y. S. Xu, 2009: An update on the wind power input to the surface geostrophic flow of the World Ocean. *Deep-Sea Res. I*, **56**, 295–304, doi:10.1016/j.dsr.2008.09.010.
- , J. A. Goff, A. C. Naveira Garabato, and A. J. Nurser, 2011: Global rate and spectral characteristics of internal gravity wave generation by geostrophic flow over topography. *J. Geophys. Res.*, **116**, C09029, doi:10.1029/2011JC007005.
- Sen, A., R. B. Scott, and B. K. Arbic, 2008: Global energy dissipation rate of deep-ocean low-frequency flows by quadratic bottom boundary layer drag: Computations from current-meter data. *Geophys. Res. Lett.*, **35**, L09606, doi:10.1029/2008GL033407.
- Sheen, K. L., and Coauthors, 2013: Rates and mechanisms of turbulent dissipation and mixing in the Southern Ocean: Results from the Diapycnal and Isopycnal Mixing Experiment in the Southern Ocean (DIMES). *J. Geophys. Res. Oceans*, **118**, 2774–2792, doi:10.1002/jgrc.20217.
- Sloyan, B. M., 2005: Spatial variability of mixing in the Southern Ocean. *Geophys. Res. Lett.*, **32**, L18603, doi:10.1029/2005GL023568.
- Sokolov, A. P., C. E. Forest, and P. H. Stone, 2003: Comparing oceanic heat uptake in AOGCM transient climate change experiments. *J. Climate*, **16**, 1573–1582, doi:10.1175/1520-0442-16.10.1573.
- Stanley, G., and O. A. Saenko, 2014: Bottom-enhanced diapycnal mixing driven by mesoscale eddies: Sensitivity to wind energy supply. *J. Phys. Oceanogr.*, **44**, 68–85, doi:10.1175/JPO-D-13-0116.1.
- St. Laurent, L. C., and C. Garrett, 2002: The role of internal tides in mixing the deep ocean. *J. Phys. Oceanogr.*, **32**, 2882–2899, doi:10.1175/1520-0485(2002)032<2882:TROI>2.0.CO;2.
- , H. L. Simmons, and S. R. Jayne, 2002: Estimating tidally driven mixing in the deep ocean. *Geophys. Res. Lett.*, **29**, 2106, doi:10.1029/2002GL015633.
- , A. C. Naveira Garabato, J. R. Ledwell, A. M. Thurnherr, J. M. Toole, and A. J. Watson, 2012: Turbulence and diapycnal mixing in Drake Passage. *J. Phys. Oceanogr.*, **42**, 2143–2152, doi:10.1175/JPO-D-12-027.1.
- Talley, L. D., 2013: Closure of the global overturning circulation through the Indian, Pacific, and Southern Oceans: Schematics and transports. *Oceanography*, **26**, 80–97, doi:10.5670/oceanog.2013.07.
- Taylor, G. I., 1915: Eddy motion in the atmosphere. *Philos. Trans. Roy. Soc. London*, **215A**, 1–26, doi:10.1098/rsta.1915.0001.
- Trossman, D. S., B. K. Arbic, S. T. Garner, J. A. Goff, S. R. Jayne, E. J. Metzger, and A. J. Wallcraft, 2013: Impact of parameterized lee wave drag on the energy budget of an eddy global ocean model. *Ocean Modell.*, **72**, 119–142, doi:10.1016/j.ocemod.2013.08.006.
- Waterman, S., A. C. Naveira Garabato, and K. L. Polzin, 2013: Internal waves and turbulence in the Antarctic Circumpolar Current. *J. Phys. Oceanogr.*, **43**, 259–282, doi:10.1175/JPO-D-11-0194.1.
- Wright, C. J., R. B. Scott, P. Ailliot, and D. Furnival, 2014: Lee wave generation rates in the deep ocean. *Geophys. Res. Lett.*, **41**, 2434–2440, doi:10.1002/2013GL059087.
- Wunsch, C., 1998: The work done by the wind on the oceanic general circulation. *J. Phys. Oceanogr.*, **28**, 2332–2340, doi:10.1175/1520-0485(1998)028<2332:TWDBTW>2.0.CO;2.
- , and R. Ferrari, 2004: Vertical mixing, energy and the general circulation of the oceans. *Annu. Rev. Fluid Mech.*, **36**, 281–314, doi:10.1146/annurev.fluid.36.050802.122121.
- Zhai, X., H. L. Johnson, and D. P. Marshall, 2010: Significant sink of ocean-eddy energy near western boundaries. *Nat. Geosci.*, **3**, 608–612, doi:10.1038/ngeo943.